

Nonlinear optimal and multi-loop flatness-based control for dual-UAV cooperative load transportation

Gerasimos Rigatos^{a,*}

M. Abbaszadeh^b

Pierluigi Siano^c

^aUnit of Industrial Automation
Industrial Systems Institute
26504, Rion Patras Greece
e-mail: grigat@ieee.org

^bDept. ECS Engineering
Rensselaer Polytechnic Institute
12065, New York, USA
e-mail: masouda@ualberta.ca

^cDept. of Innovation Systems
University of Salerno
Fisciano, 84084, Italy
e-mail: psiano@unisa.it

Mohammed AL-Numay^d

G. Cuccurullo^e

Z. Gao^f

^dDept. of Electrical Eng.
King Saud University
Riyadh 11421, Saudi Arabia
e-mail: alnumay@ksu.edu.sa

^eDept. of Industrial Eng.
University of Salerno
Fisciano, 84084, Italy
e-mail: gcuccurullo@unisa.it

^fDept. of Electrical Eng.
Univ. of Northumbria
NE1 8ST, Newcastle, UK
e-mail: zhiwei.gao@northumbria.ac.uk

Abstract: The nonlinear control problem of quadrotor UAVs which perform cooperative transportation of payloads is treated with the use of nonlinear optimal and multi-loop flatness-based control methods. The load is suspended with a link from a cart which is turn in connected through cables with two quadrotors. The aim is to compute the flight path and the control inputs of the quadrotors that will allow to lift the load and move it to any desirable final position. First, the dynamic model of the cable-suspended load is obtained through Euler-Lagrange analysis. Despite underactuation the associated nonlinear optimal control problem is solved, thus allowing to compute the lift forces of the cables that enable the load to move on the vertical plane until it reaches the targeted position. These forces are also applied with opposite sign to the quadrotors' side through joints at the other end of the cables. Thus, the dynamic model of the quadrotors is updated by including in it additional drag forces which are due to the tension of the cables. The flight paths for the two quadrotors that enables to bring the suspended load to its final position are also computed. Next, for each quadrotor the nonlinear control and path following problem is solved, taking into account the cable-induced drag forces effects. To this end, a flatness-based control approach which is implemented in successive loops is applied to each quadrotor. The state-space model of each quadrotor UAV is separated into subsystems, which are connected between them in cascading loops. Each one of these subsystems can be viewed independently as a differentially flat system and control about it can be performed with inversion of its dynamics as in the case of input-output linearized flat systems. The state variables of the second subsystem become virtual control inputs for the first subsystem. In turn, exogenous control inputs are applied to the second subsystem. The whole control method is implemented in two successive loops and its global stability properties are also proven through Lyapunov stability analysis. The whole procedure is repeated at each sampling instance, that is (i) solution of the nonlinear optimal control problem for the transportation of the payload (ii) computation of the drag forces which are exerted on the UAVs due to lifting the load, (iii) solution of the multi-loop flatness-based control problem for the individual UAVs. This control method allows each quadrotor to follow precisely the defined flight path and finally achieves to bring the load to the targeted position.

*Corresponding author

Keywords: UAV collaborative load transportation, cable-suspended load, nonlinear optimal control, autonomous quadrotors, differential flatness properties, flatness-based control in successive loops, global stability, Lyapunov analysis, path tracking.

1 Introduction

The control problem for multi-UAV payload transportation is related with several civilian, construction and defence applications where there is need to transport with the use of rotorcrafts equipment, ammunition and various types of loads and supplies to remote and difficultly accessible sites. This problem is nontrivial due to the complex nonlinear dynamics and underactuation of the integrated system which consists of the cable-suspended load and of the drones that lift the load. So far there have been several attempts to treat the nonlinear control problem of multi-UAV cooperative transportation of cable-suspended payloads. In [1] the control problem of formations of UAVs for load transportation is treated. In [2] the problem of synchronized UAVs motion in cooperative payload transportation is analyzed. In [3] and in [4] adaptive control schemes are proposed for the synchronization of multiple UAVs which transport a load. In [5] and in [6] Lyapunov theory-based controllers are used for a multi-UAV payload transportation systems. In [7] the problem of precise flight path following is treated in load transfer by multiple UAVs. In [8] a LQR-PID control scheme is proposed for the problem of the cooperative payload transportation by a swarm of UAVs. In [9] an algorithm is developed for defining the control effort (power distribution) of the UAVs in a dual-drone payload lifting and transfer system. In [10] and in [11] inverse dynamics controllers are proposed for compensating the cable-induced drag forces acting on the UAVs that lift the load. In [12] and in [13] task and path planning problems are managed aiming at synchronization of the drones that participate in coordinated lifting and transfer of loads. In [14] and in [16] multi-loop control schemes using the LQR technique are presented for the multi-UAV load transportation system. In [15] a PID controller-based multi-loop control scheme is proposed for the problem of coordinated transportation of payloads by multiple UAVs. In [17] the coordinated load transportation problem by multiple UAVs is treated within a multi-loop scheme and with the use of Lyapunov stability theory. In [18] a first control loop is used for positioning of the payload and a second control loop is applied for precise path following by the UAVs. In [19] and in [20] Euler-Lagrange analysis is used to model the multi-UAV payload transportation system and an inverse dynamics controller is proposed about it. In [21] a multi-loop control approach is developed for multi-UAV cooperative lifting and transfer of payloads. In [22] the coordinated transportation problem of a load by multiple UAVs is treated with the use of related kinematic models. In [23] cooperative payload positioning by a swarm of UAVs is implemented using multiple loops of sliding-mode controllers. In [24] dynamic modelling of the payload and the drones is performed and the precise positioning problem of the load is managed using cooperating control loops. In [25] a method is developed for distributing to the UAVs the lift forces needed for the payload's transportation. Finally, in [26] and in [27] a multi-loop control scheme based on the LMI technique is used for the multi-UAV cooperative load transportation problem,

In this article a novel method is proposed for control of dual-UAV-based cooperative transportation of payloads. This aerial load transportation system consists of a cart which is lifted by two cables while a payload is suspended from the cart with the use of a third cable, In turn the free end of each cable is pulled by a quadrotor UAV. The aim is to find forces of the cables which can move the payload to the desirable final position, and to use the tensions of the cables to compute the control inputs that should be applied to the UAVs for accomplishing the load's transportation task. At a first stage the nonlinear optimal control problem is solved for the cable-driven payload, which allows to compute the optimal forces of the cables that can bring the payload to the targeted final position [28-30]. The dynamic model of the cable-driven payload undergoes approximate linearization with the use of first-order Taylor series expansion and through the computation of the associated Jacobian matrices [31-33]. The linearization takes place at each sampling instance around the temporary operating point which is defined by the present value of the state vector of the cable-suspended payload and by the value of the control inputs vector (the cables'

tension vector) in the last sampling interval. For the approximately linearized model of the cable-driven payload an H-infinity controller is designed. To find the feedback gains and to compute the control signals of the H-infinity controller an algebraic Riccati equation is being solved in each sampling period. The global stability properties of the H-infinity controller are proven through Lyapunov analysis, which comes to ensure that if the optimal control inputs are applied to the cable-lifted payload then this load will be successfully transported to any desirable final position [34-35].

At a second stage, the problem of controlling the transportation of the payload through the cables' forces is turned into the problem of precise flight-path tracking by the UAVs that pull the load with simultaneous compensation of the cable-induced drag forces. To solve the problem of exact trajectory tracking of the UAVs under cable-induced drag forces a multi-loop flatness-based control scheme is applied. Differential flatness theory is currently one of the main research directions in the area of nonlinear control [36-40]. Briefly, a system is considered to be differentially flat if all its state variables and control inputs can be expressed as differential functions of a subset of its state vector elements which are the flat outputs [41-44]. A common form of flatness-based controllers is based on transformations of the controlled system into the canonical Brunovsky form through successive differentiations of its flat outputs [45- 49]. In the present article's approach, the state-space model of the 6-DOF autonomous quadrotors is separated into two subsystems, which are connected between them in cascading loops. By proving that differential flatness properties hold for each one of these subsystems it is confirmed that a stabilizing feedback controller can be designed for each one of them through inversion of their dynamics [50-55] . The state vector of the subsequent (i+1-th) subsystem becomes virtual control input to the preceding (i-th) subsystem. Equivalently, the virtual control input of the preceding (i-th) subsystem becomes setpoint for the subsequent (i+1-th) subsystem. From the last subsystem one computes the real control inputs which should be applied to this aerial drone by tracing backwards the virtual control inputs for all previous subsystems. The global stability properties of the drones' control scheme are proven through Lyapunov analysis. The method is easy to implement since to stabilize the load-lifting UAV it suffices to define for each one of its subsystems a positive diagonal gain matrix.

Through the article's developments it is concluded that in aggregate the nonlinear optimal and multi-loop flatness-based control scheme for dual UAV cooperative transportation of payloads ensures safe transfer and precise final positioning of the payload at any point in the drones' operating space. The quadrotors may have different dynamic models while the lengths of the cables may also be uneven. The structure of the paper is as follows: in Section 2 the dynamic model of the cable-driven payload is presented and the associated state-space model is formulated. In Section 3 the dynamic model of the 6-DOF autonomous quadrotors which lift the cable-suspended payload is analyzed and the associated state-space model is formulated. In Section 4 a nonlinear optimal control method is developed for computing the cables' forces which can safely transport the payload to the targeted final position. The global stability properties of the payload control scheme are proven through Lyapunov analysis. In Section 5 the tensions of the cables which have been computed through the solution of the above-noted optimal control problem are considered to be drag forces for the drones. A multi-loop flatness-based control method is developed for computing the control inputs which enable precise flight-path tracking by the load-lifting UAVs and simultaneous compensation of cable-induced drag forces. The global stability properties of the drones' control scheme are proven through Lyapunov analysis. In Section 6 Simulation experiments are performed to confirm that the proposed nonlinear optimal and multi-loop flatness-based control method ensures the desirable performance for the dual-UAV payload transportation system. The payload is shown to be precisely placed to any targeted final position after computing the optimal cable tensions that should be applied on it, while the two quadrotors are shown to follow precisely their flight trajectories with simultaneous rejection of the cable-induced drag forces on the side of the load-lifting UAVs.

2 Dynamic model of the cable-driven payload

2.1 State-space model of the cable-driven payload

The diagram of the dual-UAV cooperative load transportation system, consisting of the cable-suspended payload which is lifted by two quadrotor UAVs is shown in Fig. 1. This load consists of a cart which is moved on a 2D yz -plane with the use of two cables which in turned are pulled by two UAVs. Considering motion of the cart only on the vertical yz plane results into a lower dimensionality and numerically simpler control problem. In the 2D case, the position of the cart in the yz -plane is denoted as (y_R, z_R) . The position of the left UAV is denoted as (y_a, z_a) while the position of the right UAV is described as (y_b, z_b) . The mass of the cart is M . The length of the cable that connects the cart with the left UAV is denoted as L_1 , while the length of the cable which connects the cart with the right UAV is denoted as L_2 . Besides, a load of mass m is suspended from the cart using an unactuated link of length L_3 . The angle which is formed between the OY horizontal axis and the cable that connects the cart to the left UAV is denoted as a_1 . The angle which is formed between the OY horizontal axis and the cable that connects the cart to the right UAV is denoted as a_2 .

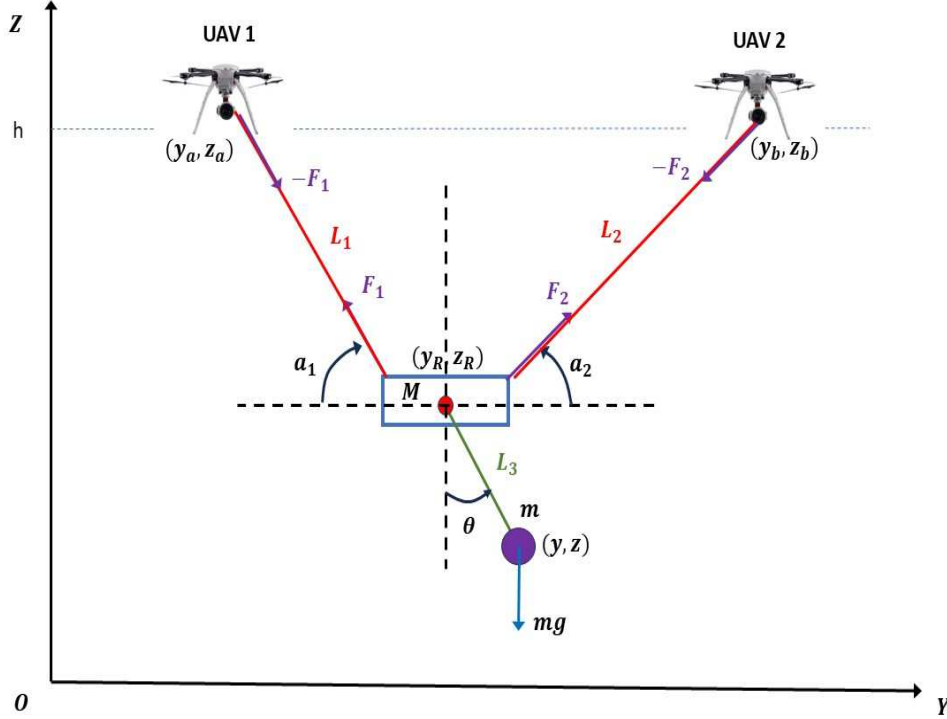


Figure 1: Diagram of the dual-UAV cooperative payload transportation system, consisting of the cable-suspended payload which is lifted by two quadrotor UAVs

The dynamic model of the two UAVs is the one of 6-DOF quadrotors and is given in Section 3. The cables are considered to be massless and inelastic. The link which connects the load of mass m to the cart is not subject to deformation either. The parameters which describe the motion of the cable-suspended payload constitute the parameters' vector $[y_R, z_R, \theta]^T$, while the control objective is to make this vector

converge fast to the desirable value $[y_{R,d}, z_{R,d}, \theta_d]^T$ under lift forces which will be provided by the two UAVs.

Using trigonometric relations the following geometric constraints are given:

$$\begin{aligned} (y_a - y_R)^2 + (z_a - z_R)^2 &= L_1^2 \\ (y_b - y_R)^2 + (z_b - z_R)^2 &= L_2^2 \end{aligned} \quad (1)$$

To perform Euler-Lagrange analysis for the load its kinetic and dynamic energy are computed first. The position of the cart is (y_R, z_R) thus the associated velocity is (\dot{y}_R, \dot{z}_R) . The position of the payload is $(y_R + L_3 \sin(\theta), z_R - L_3 \cos(\theta))$ and the associated velocity is $(\dot{y}_R + L_3 \cos(\theta)\dot{\theta}, \dot{z}_R + L_3 \sin(\theta)\dot{\theta})$.

The dynamic model of the system will be defined using Euler-Lagrange analysis [28]. The kinetic energy of the cart is

$$K_c = \frac{1}{2}M(\dot{y}_R^2 + \dot{z}_R^2) \quad (2)$$

The kinetic energy of the load is

$$K_L = \frac{1}{2}m[(\dot{y}_R + L_3 \cos(\theta)\dot{\theta})^2 + (\dot{z}_R + L_3 \sin(\theta)\dot{\theta})^2] \quad (3)$$

The aggregate kinetic energy of the crane is

$$\begin{aligned} K &= K_c + K_L \Rightarrow K = \frac{1}{2}M(\dot{y}_R^2 + \dot{z}_R^2) + \\ &+ \frac{1}{2}m[(\dot{y}_R + L_3 \cos(\theta)\dot{\theta})^2 + (\dot{z}_R + L_3 \sin(\theta)\dot{\theta})^2] \end{aligned} \quad (4)$$

which after intermediate operations and regrouping of terms gives

$$\begin{aligned} K &= \frac{1}{2}(M + m)\dot{y}_R^2 + \frac{1}{2}(M + m)\dot{z}_R^2 + \\ &+ m\dot{y}_R L_3 \cos(\theta)\dot{\theta} + m\dot{z}_R L_3 \sin(\theta)\dot{\theta} + \frac{1}{2}mL_3^2\dot{\theta}^2 \end{aligned} \quad (5)$$

By defining vector $q = [y_R, z_R, \theta]^T$ and vector $\dot{q} = [\dot{y}_R, \dot{z}_R, \dot{\theta}]^T$, the kinetic energy of the cable-suspended payload can be written in matrix form as

$$K = \frac{1}{2}\dot{q}^T \tilde{M} \dot{q} \Rightarrow K = \frac{1}{2}(\dot{y}_R, \dot{z}_R, \dot{\theta}) \begin{pmatrix} (M + m) & 0 & mL_3 \cos(\theta) \\ 0 & (M + m) & mL_3 \sin(\theta) \\ mL_3 \cos(\theta) & mL_3 \sin(\theta) & mL_3^2 \end{pmatrix} \begin{pmatrix} \dot{y}_R \\ \dot{z}_R \\ \dot{\theta} \end{pmatrix} \quad (6)$$

Next, the potential energy of the crane, consisting of the potential energy of the cart and the potential energy of the payload, is found to be

$$P = Mgz_R + mg(z_R - L_3 \cos(\theta)) \quad (7)$$

The Lagrangian of the crane is given by

$$\begin{aligned} L &= K - P \Rightarrow L = \frac{1}{2}(M + m)\dot{y}_R^2 + \frac{1}{2}(M + m)\dot{z}_R^2 + \\ &+ m\dot{y}_R L_3 \cos(\theta)\dot{\theta} + m\dot{z}_R L_3 \sin(\theta)\dot{\theta} + \frac{1}{2}mL_3^2\dot{\theta}^2 - \\ &- Mgz_R - mg(z_R - L_3 \cos(\theta)) \end{aligned} \quad (8)$$

The forces which are exerted on the load are the tensions of the two string F_1 and F_2 , while there is no torque. By applying Euler-Lagrange analysis one obtains:

$$\frac{\partial}{\partial t} \frac{\partial L}{\partial \dot{q}_1} - \frac{\partial L}{\partial q_1} = F_1 \quad (9)$$

$$\frac{\partial}{\partial t} \frac{\partial L}{\partial \dot{q}_2} - \frac{\partial L}{\partial q_2} = F_2 \quad (10)$$

$$\frac{\partial}{\partial t} \frac{\partial L}{\partial \dot{q}_3} - \frac{\partial L}{\partial q_3} = 0 \quad (11)$$

From Eq. (9) and after computing the related partial derivatives of the Lagrangian one gets:

$$(M + m)\ddot{y}_R - mL_3\sin(\theta)\dot{\theta}^2 + mL_3\cos(\theta)\ddot{\theta} = F_1 \quad (12)$$

$$(M + m)\ddot{z}_R + mL_3\cos(\theta)\dot{\theta}^2 + mL_3\sin(\theta)\ddot{\theta} - (M + m)g = F_2 \quad (13)$$

$$m\ddot{y}_RL_3\cos(\theta) + m\ddot{z}_RL_3\sin(\theta) + mL_3^2\ddot{\theta} + mgL_3\sin(\theta) - m\dot{y}_RL_3\sin(\theta)\dot{\theta} + m\dot{z}_RL_3\cos(\theta)\dot{\theta} = 0 \quad (14)$$

In Eq. (14) the terms which appear in the last row are zero, that is it holds $-m\dot{y}_RL_3\sin(\theta)\dot{\theta} + m\dot{z}_RL_3\cos(\theta)\dot{\theta} = 0$ or $mL_3\dot{\theta}[-\dot{y}_R\sin(\theta) + \dot{z}_R\cos(\theta)] = 0$. Actually, it holds that $-\dot{y}_R\sin(\theta) + \dot{z}_R\cos(\theta) = 0$. This is obtained after considering a body-fixed frame for expressing the velocity of the load and knowing that the velocity of the load along the vertical axis of this frame is 0. Indeed, the transformation of the velocities vector of the load from the inertial reference frame to the body-fixed frame gives

$$\begin{pmatrix} v_1 \\ 0 \end{pmatrix} = \begin{pmatrix} \cos(\theta) & \sin(\theta) \\ -\sin(\theta) & \cos(\theta) \end{pmatrix} \begin{pmatrix} \dot{y}_R + L_3\cos(\theta)\dot{\theta} \\ \dot{z}_R + L_3\sin(\theta)\dot{\theta} \end{pmatrix} \quad (15)$$

out of which one obtains

$$\begin{aligned} -\sin(\theta)[\dot{y}_R + L_3\cos(\theta)\dot{\theta}] + \cos(\theta)[\dot{z}_R + L_3\sin(\theta)\dot{\theta}] &= 0 \\ \Rightarrow -\dot{y}_R\sin(\theta) + \dot{z}_R\cos(\theta) &= 0 \end{aligned} \quad (16)$$

Consequently, from Euler-Lagrange analysis the equations of the system's dynamics become

$$(M + m)\ddot{y}_R + 0\ddot{z}_R - mL_3\sin(\theta)\dot{\theta}^2 + mL_3\cos(\theta)\ddot{\theta} = F_1 \quad (17)$$

$$0\ddot{y}_R + (M + m)\ddot{z}_R + mL_3\cos(\theta)\dot{\theta}^2 + mL_3\sin(\theta)\ddot{\theta} - (M + m)g = F_2 \quad (18)$$

$$m\ddot{y}_RL_3\cos(\theta) + m\ddot{z}_RL_3\sin(\theta) + mL_3^2\ddot{\theta} + mgL_3\sin(\theta) = 0 \quad (19)$$

In matrix form the dynamic model of the two cable-driven 3-DOF load is written as:

$$\begin{pmatrix} (M + m) & 0 & (mL_3\cos(\theta)) \\ 0 & (M + m) & (mL_3\sin(\theta)) \\ (mL_3\cos(\theta)) & (mL_3\sin(\theta)) & mL_3^2 \end{pmatrix} \begin{pmatrix} \ddot{y} \\ \ddot{z} \\ \ddot{\theta} \end{pmatrix} + \begin{pmatrix} -(mL_3\sin(\theta))\dot{\theta}^2 \\ (mL_3\cos(\theta))\dot{\theta}^2 \\ 0 \end{pmatrix} + \begin{pmatrix} 0 \\ 0 \\ mgL_3\cos(\theta) \end{pmatrix} = \begin{pmatrix} F_1 \\ \bar{F}_2 \\ 0 \end{pmatrix} \quad (20)$$

where $\bar{F}_2 = F_2 + (M + m)g$. Using that $q = [y_R, z_R, \theta]^T$, this is a dynamic model of a rigid body that performs a 3-DOF motion, with an inertia matrix $M(q) \in R^{3 \times 3}$, a Coriolis forces vector $C(q, \dot{q}) \in R^{3 \times 1}$, gravitational forces vector $G(\theta) \in R^{3 \times 1}$, and external (control input) forces/torques vector $\tau \in R^{3 \times 3}$. This dynamic model can be written in the concise form

$$M(q)\ddot{q} + C(q, \dot{q}) + G(q) = \tau \quad (21)$$

The inverse of the inertia matrix $M(q)$ is computed as follows:

$$M(q)^{-1} = \frac{1}{\det M} \begin{pmatrix} M_{11} & -M_{12} & M_{13} \\ -M_{21} & M_{22} & -M_{23} \\ M_{31} & -M_{32} & M_{33} \end{pmatrix} \quad (22)$$

where the sub-determinants of $M(q)$ are: $M_{11} = (M+m)mL_3^2 - (mL_3 \sin(\theta))^2$, $M_{12} = -(mL_3)^2 \sin(\theta) \cos(\theta)$, $M_{13} = -(M+m)(mL_3 \cos(\theta))$, $M_{21} = -(mL_3)^2 \sin(\theta) \cos(\theta)$, $M_{22} = (M+m)mL_3^2 - (mL_3 \cos(\theta))^2$, $M_{23} = (M+m)(mL_3 \cos(\theta))$, $M_{31} = -(M+m)(mL_3 \cos(\theta))$, $M_{32} = (M+m)(mL_3 \sin(\theta))$ and $M_{33} = (M+m)^2$ while the determinant of $M(q)$ is $\det M = (M+m)M_{11} + (mL_3 \cos(\theta))M_{13}$.

The Coriolis forces vector is written as $C = [C_1, C_2, 0]^T$ and the gravitational forces vector is written as $G[0, 0, G_3]^T$. Thus, after some intermediate operations the dynamic model of the payload is written as

$$\begin{pmatrix} \ddot{y}_R \\ \ddot{z}_R \\ \ddot{\theta} \end{pmatrix} = -\frac{1}{\det M} \begin{pmatrix} M_{11} & -M_{21} & M_{31} \\ -M_{12} & M_{22} & -M_{32} \\ M_{13} & -M_{23} & M_{33} \end{pmatrix} \begin{pmatrix} C_1 \\ C_2 \\ G_3 \end{pmatrix} + \frac{1}{\det M} \begin{pmatrix} M_{11} & -M_{21} & M_{31} \\ -M_{12} & M_{22} & -M_{32} \\ M_{13} & -M_{23} & M_{33} \end{pmatrix} \begin{pmatrix} F_1 \\ \bar{F}_2 \\ 0 \end{pmatrix} \quad (23)$$

which finally gives

$$\begin{pmatrix} \ddot{y}_R \\ \ddot{z}_R \\ \ddot{\theta} \end{pmatrix} = \begin{pmatrix} \frac{-M_{11}C_1 + M_{21}C_2 - M_{31}G_3}{\det M} \\ \frac{M_{12}C_1 - M_{22}C_2 + M_{32}G_3}{\det M} \\ \frac{-M_{13}C_1 + M_{23}C_2 - M_{33}G_3}{\det M} \end{pmatrix} + \frac{1}{\det M} \begin{pmatrix} \frac{M_{11}}{\det M} & -\frac{M_{21}}{\det M} \\ -\frac{M_{12}}{\det M} & \frac{M_{22}}{\det M} \\ \frac{M_{13}}{\det M} & -\frac{M_{23}}{\det M} \end{pmatrix} \begin{pmatrix} F_1 \\ \bar{F}_2 \end{pmatrix} \quad (24)$$

Next, the state vector of the load is defined as $x = [x_1, x_2, x_3, x_4, x_5, x_6]^T$ or $x = [y_R, \dot{y}_R, z_R, \dot{z}_R, \theta, \dot{\theta}]^T$, and the control inputs vector is defined as $u = [u_1, u_2]^T$ or $u = [F_1, \bar{F}_2]^T$. Thus, the dynamic model of the cable-suspended payload is written as

$$\begin{pmatrix} \dot{x}_1 \\ \dot{x}_2 \\ \dot{x}_3 \\ \dot{x}_4 \\ \dot{x}_5 \\ \dot{x}_6 \end{pmatrix} = \begin{pmatrix} x_2 \\ \frac{-M_{11}C_1 + M_{21}C_2 - M_{31}G_3}{\det M} \\ x_4 \\ \frac{M_{12}C_1 - M_{22}C_2 + M_{32}G_3}{\det M} \\ x_6 \\ \frac{-M_{13}C_1 + M_{23}C_2 - M_{33}G_3}{\det M} \end{pmatrix} + \begin{pmatrix} 0 & 0 \\ \frac{M_{11}}{\det M} & -\frac{M_{21}}{\det M} \\ 0 & 0 \\ -\frac{M_{12}}{\det M} & \frac{M_{22}}{\det M} \\ 0 & 0 \\ \frac{M_{13}}{\det M} & -\frac{M_{23}}{\det M} \end{pmatrix} \begin{pmatrix} u_1 \\ u_2 \end{pmatrix} \quad (25)$$

or equivalently the load's dynamics can be written in the nonlinear affine-in-the-input state-space form

$$\dot{x} = f(x) + g(x)u \quad (26)$$

$x \in R^{6 \times 1}$, $f(x) \in R^{6 \times 1}$, $g(x) \in R^{6 \times 1}$ and $u \in R^{2 \times 1}$. Nonlinear dynamics and underactuation make the solution of the associated control problem be a nontrivial task.

2.2 Differential flatness properties of the cable-driven payload

It will be proven that the dynamic model of the two cable-driven 3-DOF payload is differentially flat, with flat outputs vector $Y = (y_R, z_R)^T$. It holds that

$$\begin{aligned} x_2 = \dot{x}_1 &\Rightarrow x_2 = h_2(Y, \dot{Y}) \\ x_4 = \dot{x}_3 &\Rightarrow x_4 = h_4(Y, \dot{Y}) \end{aligned} \quad (27)$$

which signifies that state variables x_2, x_4 are differential functions of the flat outputs of the system. Besides from the condition of Eq. (16) it holds that

$$\begin{aligned} -\sin(\theta)\dot{y}_R + \cos(\theta)\dot{z}_R = 0 &\Rightarrow \tan(\theta) = \frac{\dot{z}_R}{\dot{y}_R} \Rightarrow \theta = \tan^{-1}\left(\frac{\dot{z}_R}{\dot{y}_R}\right) \\ &\Rightarrow x_5 = \tan^{-1}\left(\frac{\dot{z}_R}{\dot{y}_R}\right) \Rightarrow x_5 = h_5(Y, \dot{Y}) \end{aligned} \quad (28)$$

$$x_6 = \dot{x}_5 \Rightarrow x_6 = h_6(Y, \dot{Y})$$

which signifies that state variables x_5 and x_6 are also differential functions of the flat outputs of the system. Next, one uses Eq. (24) which in concise form is written as

$$\ddot{q} = \tilde{F}(q, \dot{q}) + \tilde{G}(q)u \quad (29)$$

Using the Moore-Penrose matrix of $\tilde{G}(q)$ one obtains

$$u = [\tilde{G}^T(q)\tilde{G}(q)]^{-1}\tilde{G}^T(q)[\ddot{q} - \tilde{F}(q, \dot{q})] \quad (30)$$

where $q = [y_R, z_R, \theta]^T$. Thus, it is confirmed that the control inputs vector $u = [u_1, u_2]^T$ is a differential function of the flat outputs vector, or

$$u_1 = h_{u_1}(Y, \dot{Y}) \quad u_2 = h_{u_2}(Y, \dot{Y}) \quad (31)$$

The proof of differential flatness properties for the load's model is an implicit proof of this system's controllability. Besides, it allows to treat the setpoints definition problem. One selects setpoints without constraints for state variables $x_1 = y_R$ and $x_3 = z_R$ which are associated with the flat outputs of the system. For state variable θ , setpoints can be chosen using the differential relation which connects this variable with the flat output $\theta_d = \tan^{-1}(\frac{\dot{z}_R}{\dot{y}_R})$. At steady-state it holds $\theta_d = 0$.

3 Dynamic model of the 6-DOF autonomous quadrotors

The considered problem is that of control of the quadrotor in a 6 degrees of freedom motion, with simultaneous compensation of the cable-induced drag forces. The first three degrees of freedom describe translational motion of the quadrotor in the xyz cartesian space, along the x-axis, the y-axis and the z-axis, as shown in Fig. 2. The rest three degrees of freedom describe rotational motion of the quadrotor around the axes of the inertial reference frame. Considering as state variables (a) the x , y and z -axis position of the UAV, (b) the rotation angles of the drone ϕ , θ and ψ around the axes of the inertial reference frame, (c) the linear angular velocities of the UAV \dot{x} , \dot{y} and \dot{z} along the axes of inertial frame and finally (d) the angular velocities of the UAV $\dot{\phi}$, $\dot{\theta}$, and $\dot{\psi}$ around the axes of the inertial coordinates system, the resulting state-space model is of dimension 12, while receiving only four control inputs. The four control inputs of the quadrotor are a thrust force that can lift up the drone and torques generated by the unequal turn speeds of its rotors that can change the position of the quadrotor's center of gravity or can change its orientation angles with respect to the axes of the inertial reference frame. The quadrotor's model is nonlinear and underactuated and the solution of the associated control problem is a nontrivial task.

The kinematic and dynamic model of the quadrotor can be described with the use of a body-fixed frame and an inertial reference frame. The body-fixed frame is denoted as $OXYZ$ and describes the position of the quadrotor in the cartesian space $\xi = [x, y, z]^T$, as well as the quadrotor's attitude which is described by the Euler angles vector $\eta = [\phi, \theta, \psi]^T$ (rotation angles around axes OX, OY and OZ respectively). The body-fixed frame is denoted as $OB_1B_2B_3$ and describes linear velocities $V_B = [u, v, w]^T$, as well as rotation velocities $\omega = [p, q, r]^T$ in this coordinates system [36], [28].

The linear velocities vector of the quadrotor in the inertial frame is denoted by $V_E = [\dot{x}, \dot{y}, \dot{z}]^T$ and is related with the velocities vector in the body-fixed frame $V_B = [u, v, w]^T$ through the following equation [36], [28]

$$V_E = RV_B \quad (32)$$

where rotation matrix R is given by

$$R = \begin{pmatrix} C\psi C\theta & C\psi S\theta S\phi - S\psi C\phi & C\psi S\theta C\phi + S\psi S\phi \\ S\psi C\theta & S\psi S\theta S\phi + C\psi C\phi & S\psi S\theta C\phi - C\psi S\phi \\ -S\theta & C\theta S\phi & C\theta C\phi \end{pmatrix} \quad (33)$$

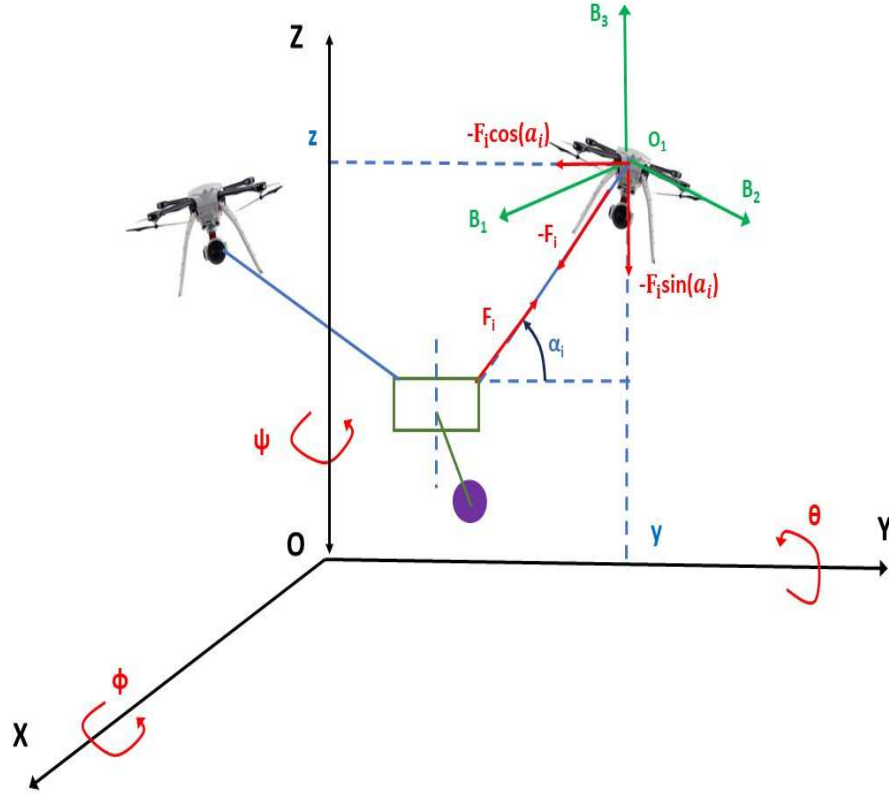


Figure 2: Inertial and body-fixed reference frames and forces due to tension of the cable at the i -th drone when transporting the payload in the vertical OYZ plane

where $C = \cos(\cdot)$ and $S = \sin(\cdot)$. The angular velocities of the quadrotor in the inertial frame $\dot{\eta} = [\dot{\phi}, \dot{\theta}, \dot{\psi}]^T$ and the angular velocities in the body-fixed frame $\omega = [p, q, r]^T$ are connected through the relation

$$\dot{\eta} = W^{-1}\omega \quad (34)$$

that is [28],[36]

$$\begin{pmatrix} \dot{\phi} \\ \dot{\theta} \\ \dot{\psi} \end{pmatrix} = \begin{pmatrix} 1 & \sin(\phi)\tan(\theta) & \cos(\phi)\tan(\theta) \\ 0 & \cos(\phi) & -\sin(\phi) \\ 0 & \sin(\phi)\sec(\theta) & \cos(\phi)\sec(\theta) \end{pmatrix} \begin{pmatrix} p \\ q \\ r \end{pmatrix} \quad (35)$$

The Euler-Lagrange equation for the quadrotor is formulated as follows

$$\frac{d}{dt}\left(\frac{\partial L}{\partial \dot{q}_i}\right) - \frac{\partial L}{\partial q_i} = \begin{pmatrix} f_\xi \\ \tau_\eta \end{pmatrix} \quad (36)$$

where the Lagrangian is defined as $L(q, \dot{q}) = E_{C_{tr}} + E_{C_{rot}} - E_p$, $E_{C_{tr}}$ is the kinetic energy of the quadrotor due to translational motion, $E_{C_{rot}}$ is the kinetic energy of the quadrotor due to rotational motion and E_p is the total potential energy of the quadrotor due to lift. The generalized state vector is $q = [\xi^T, \eta^T]^T \in \mathbb{R}^6$, $\tau_\eta \in \mathbb{R}^3$ is the torques vector that causes rotation round the axes of the body-fixed reference frame, and $f_\xi = R\hat{f} + \alpha_T$ is the translational forces vector applied to the quadrotor due to the main control input

U_1 , while $\alpha_T = [A_x, A_y, A_z]^T$ is the aerodynamic forces vector, defined along the axes of the inertial reference frame. Since the Lagrangian does not contain cross-coupling between the $\dot{\xi}$ and the $\dot{\eta}$ terms, the Lagrange-Euler equations can be divided into translational and rotational dynamics. The parameters of the dynamic model of the quadrotor which is obtained from Euler-Lagrange analysis are concisely given in Table I.

Table I	
Euler-Lagrange analysis for the quadrotors	
Parameter	Definition
$L(q, \dot{q}) = E_{C_{tr}} + E_{C_{rot}} - E_p$	Lagrangian of the quadrotor
$E_{C_{tr}}$	kinetic energy due to translational motion
$E_{C_{rot}}$	kinetic energy due to rotational motion
E_p	total potential energy due to lift
$q = [\xi^T, \eta^T]^T \in R^6$	generalized state vector
$\xi \in R^3$	Cartesian coordinates vector
$\eta \in R^3$	rotation angles vector in inertial frame
$\tau_\eta \in R^3$	torques' vector
$f_\xi = R\hat{f} + \alpha_T$	translational forces vector
$\alpha_T = [A_x, A_y, A_z]^T$	aerodynamic forces vector

The translational dynamics of the quadrotor is given by

$$m\ddot{\xi} + mge_3 = f_\xi \quad (37)$$

where $e_3 = [0, 0, 1]^T$ is the unit vector along the z axis of the inertial reference frame. With reference to Fig. 2 the tension of the cable that connects the load to the drone is F , and the cable's angle with the horizontal OY axis is α . Consequently additional drag forces are applied on each drone due to the cable's tension. These are given by $F_y = -F\cos(a)$ and $F_z = -F\sin(a)$, where for the first drone one has $F = F_1$ while for the second drone of Fig. 1 it holds that $F = F_2$. Thus, for each drone Eq. (37) can be written using the following three equations [36], [28]:

$$\begin{aligned} \ddot{x} &= \frac{1}{m}(\cos(\psi)\sin(\theta)\cos(\phi) + \sin(\psi)\sin(\phi))U_1 + \frac{A_x}{m} \\ \ddot{y} &= \frac{1}{m}(\sin(\psi)\sin(\theta)\cos(\phi) - \cos(\psi)\sin(\phi))U_1 + \frac{A_y}{m} - \frac{1}{m}F\cos(a) \\ \ddot{z} &= -g + \frac{1}{m}(\cos(\theta)\cos(\phi))U_1 + \frac{A_z}{m} - \frac{1}{m}F\sin(a) \end{aligned} \quad (38)$$

where m is the quadrotor's mass and g is the gravitational acceleration. The rotational dynamics of the quadrotor is given by [36], [28]

$$M(\eta)\ddot{\eta} + C(\eta, \dot{\eta})\dot{\eta} = \tau_\eta \quad (39)$$

where the inertia matrix $M(\eta)$ is defined as

$$M(\eta) = \begin{pmatrix} I_{xx} & 0 & -I_{xx}S\theta \\ 0 & I_{yy}C^2\phi + I_{zz}S^2\phi & (I_{yy} - I_{zz})C\phi S\phi C\theta \\ -I_{xx}S\theta & (I_{yy} - I_{zz})C\phi S\phi C\theta & I_{xx}S^2\theta + I_{yy}S^2\phi C^2\theta + I_{zz}C^2\phi C^2\theta \end{pmatrix} \quad (40)$$

and the Coriolis matrix is

$$C(\eta, \dot{\eta}) = \begin{pmatrix} c_{11} & c_{12} & c_{13} \\ c_{21} & c_{22} & c_{23} \\ c_{31} & c_{32} & c_{33} \end{pmatrix} \quad (41)$$

where the elements of the matrix are

$$\begin{aligned}
c_{11} &= 0 \\
c_{12} &= (I_{yy} - I_{zz})(\dot{\theta}C\phi S\phi + \dot{\psi}S^2\phi C\theta) + (I_{zz} - I_{yy})\dot{\psi}C^2\phi C\theta \\
c_{13} &= (I_{zz} - I_{yy})\dot{\psi}C\phi S\phi C^2\theta \\
c_{21} &= (I_{zz} - I_{yy})(\dot{\theta}C\phi S\phi + \dot{\psi}S^2\phi C\theta) + (I_{yy} - I_{zz})\dot{\psi}C^2\phi C\theta + I_{xx}\dot{\psi}C\theta \\
c_{22} &= (I_{zz} - I_{yy})\dot{\phi}C\phi S\phi \\
c_{23} &= -I_{xx}\dot{\psi}S\theta C\theta + I_{yy}\dot{\psi}S^2\phi C\theta S\theta + I_{zz}\dot{\psi}C^2\phi S\theta C\theta \\
c_{31} &= (I_{yy} - I_{zz})\dot{\psi}C^2\theta S\phi C\phi - I_{xx}\dot{\theta}C\theta \\
c_{32} &= (I_{zz} - I_{yy})(\dot{\theta}C\phi S\phi S\theta + \dot{\phi}S^2\phi C\theta) + (I_{yy} - I_{zz})\dot{\phi}C^2\phi C\theta + I_{xx}\dot{\psi}S\theta C\theta - \\
&\quad - I_{yy}\dot{\psi}S^2\phi S\theta C\theta - I_{zz}\dot{\psi}C^2\phi S\theta C\theta \\
c_{33} &= (I_{yy} - I_{zz})\dot{\phi}C\phi S\phi C^2\theta - I_{yy}\dot{\theta}S^2\phi C\theta S\theta - \\
&\quad - I_{zz}\dot{\theta}C^2\phi C\theta S\theta + I_{xx}\dot{\theta}C\theta S\theta
\end{aligned} \tag{42}$$

Thus, the mathematical model that describes the quadrotor's rotational motion is given by [36], [28]

$$\ddot{\eta} = -C(\eta, \dot{\eta})\dot{\eta} + M(\eta)^{-1}\tau_{\eta} \tag{43}$$

The following variables are also introduced: $\bar{F}_y = \frac{1}{m}F\cos(a)$ and $\bar{F}_z = \frac{1}{m}F\sin(a)$. Next, in the relations describing the translational motion of the quadrotor, given in Eq. (38) one defines the following control inputs:

$$\begin{aligned}
v_1 &= \frac{1}{m}(\cos(\psi)\sin(\theta)\cos(\phi) + \sin(\psi)\sin(\phi))U_1 \\
v_2 &= -\bar{F}_y + \frac{1}{m}(\sin(\psi)\sin(\theta)\cos(\phi) - \cos(\psi)\sin(\phi))U_1 \\
v_3 &= -\bar{F}_z - g + \frac{1}{m}(\cos(\theta)\cos(\phi))U_1
\end{aligned} \tag{44}$$

After intermediate algebraic operations one can confirm that the following relations hold

$$v_1^2 + (v_2 + \bar{F}_y)^2 + (v_3 + \bar{F}_z + g)^2 = \frac{1}{m}U_1^2 \Rightarrow U_1 = m \cdot \sqrt{v_1^2 + (v_2 + \bar{F}_y)^2 + (v_3 + \bar{F}_z + g)^2} \tag{45}$$

Using the above definition of auxiliary control inputs, as well as the definition for aerodynamics coefficients $A_x = -K_x x$, $A_y = -K_y y$, $A_z = -K_z z$, the dynamics of the translational motion of the quadrotor, previously given in Eq. (38) are now written as

$$\begin{aligned}
\ddot{x} &= -\frac{K_x x}{m} + v_1 \\
\ddot{y} &= -\frac{K_y y}{m} + v_2 \\
\ddot{z} &= -\frac{K_z z}{m} + v_3
\end{aligned} \tag{46}$$

or equivalently

$$\begin{pmatrix} \ddot{x} \\ \ddot{y} \\ \ddot{z} \end{pmatrix} = \begin{pmatrix} -\frac{K_x}{m} & 0 & 0 \\ 0 & -\frac{K_y}{m} & 0 \\ 0 & 0 & -\frac{K_z}{m} \end{pmatrix} \begin{pmatrix} x \\ y \\ z \end{pmatrix} + \begin{pmatrix} 1 & 0 & 0 \\ 0 & 1 & 0 \\ 0 & 0 & 1 \end{pmatrix} \begin{pmatrix} v_1 \\ v_2 \\ v_3 \end{pmatrix} \tag{47}$$

By denoting vectors $x_E = [x, y, z]^T$, $v_E = [\dot{x}, \dot{y}, \dot{z}]^T$, $F_E = [v_1, v_2, v_3]^T$, as well as by denoting matrices $K_E = \text{diag}[-\frac{K_x}{m}, -\frac{K_y}{m}, -\frac{K_z}{m}]$, $G_E = I_{3 \times 3}$ one has the following concise description for the translational motion of the quadrotor

$$\begin{aligned}
\dot{x}_E &= V_E \\
\dot{V}_E &= K_E x_E + G_E F_E
\end{aligned} \tag{48}$$

Moreover, in the equation about the rotational motion of the quadrotor which appears in Eq. (43) one can use the vectors definition $\dot{\eta} = \omega_E = [\phi, \theta, \psi]^T$, $\ddot{\eta} = [\dot{\phi}, \dot{\theta}, \dot{\psi}]^T$, and can finally rewrite the rotational dynamics of the UAV in the form

$$\begin{aligned}\dot{\eta} &= \omega_E \\ \dot{\omega}_E &= -C(\eta, \dot{\eta})\dot{\eta} + M(\eta)^{-1}\tau_\eta\end{aligned}\quad (49)$$

Next, by merging Eq. (48) and Eq. (49) one obtains the complete dynamic model of each quadrotor in the form

$$\begin{aligned}\dot{x}_E &= V_E \\ \dot{\eta} &= \omega_E \\ \dot{V}_E &= K_E x_E + G_E F_E \\ \dot{\omega}_E &= -C(\eta, \dot{\eta})\dot{\eta} + M(\eta)^{-1}\tau_\eta\end{aligned}\quad (50)$$

Next, the state-vector of each quadrotor is defined as

$$\begin{aligned}x &= [x_E, \eta, V_E, \omega_E]^T \Rightarrow \\ x &= [x, y, z, \phi, \theta, \psi, \dot{x}, \dot{y}, \dot{z}, \dot{\phi}, \dot{\theta}, \dot{\psi}]^T \Rightarrow \\ x &= [x_1, x_2, x_3, x_4, x_5, x_6, x_7, x_8, x_9, x_{10}, x_{11}, x_{12}]^T\end{aligned}\quad (51)$$

and the control inputs vector of this UAV is defined as

$$\begin{aligned}u &= [F_E, \tau_\eta]^T \Rightarrow u = [v_1, v_2, v_3, \tau_\phi, \tau_\theta, \tau_\psi]^T \\ &\Rightarrow u = [u_1, u_2, u_3, u_4, u_5, u_6]^T\end{aligned}\quad (52)$$

Additionally, the dynamic model of each quadrotor can be written in the form of two chained subsystems after defining the state subvectors $x_{1,6} = [x_1, x_2, x_3, x_4, x_5, x_6]^T$ and $x_{7,12} = [x_7, x_8, x_9, x_{10}, x_{11}, x_{12}]^T$ as well as the following subvectors and submatrices.

$$f_{1,6}(x_{1,6}) = 0_{6 \times 1} \quad g_{1,6}(x_{1,6}) = I_{6 \times 6} \quad (53)$$

$$f_{7,12}(x_{1,6}, x_{7,12}) = \begin{pmatrix} K_E x_E \\ -M^{-1}(u)C((\eta, \omega_E)\omega_E) \end{pmatrix} \quad g_{7,12}(x_{1,6}, x_{7,12}) = \begin{pmatrix} G_E & 0 \\ 0 & M^{-1}(\eta) \end{pmatrix} \quad (54)$$

Using the above, the dynamics of each quadrotor can be written in the form of two chained subsystems

$$\dot{x}_{1,6} = f_{1,6}(x_{1,6}) + g_{1,6}(x_{1,6}, x_{7,12})x_{7,12} \quad (55)$$

$$\dot{x}_{7,12} = f_{7,12}(x_{1,6}, x_{7,12}) + g_{7,12}(x_{1,6}, x_{7,12})u \quad (56)$$

The dynamic model of the quadrotor is differentially flat with flat output vector $Y = [x_1, x_2, x_3, x_4, x_5, x_6]^T = x_{1,3}$. Indeed from Eq. (55)

$$\begin{aligned}x_{7,12} &= g_{1,6}(x_{1,6})^{-1}[\dot{x}_{1,6} - f_{1,6}(x_{1,6})] \\ &\Rightarrow x_{7,12} = h_{x_{7,12}}(Y, \dot{Y})\end{aligned}\quad (57)$$

This signifies that $x_{7,12}$ is a differential function of the flat outputs of the system Y . Moreover, from Eq. (56) one solves for the control inputs vector u . This gives

$$\begin{aligned}u &= g_{7,12}^{-1}(x_{1,6}, x_{7,12})[\dot{x}_{7,12} - f_{7,12}(x_{1,6}, x_{7,12})] \\ &\Rightarrow u = h_u(Y, \dot{Y})\end{aligned}\quad (58)$$

which signifies that u is a differential function of the flat outputs vector. Consequently, the dynamic model of each quadrotor is differentially flat.

4 Nonlinear optimal control for the cable-suspended payload

4.1 Approximate linearization of two cable-driven payload

The dynamic model of the two cable-driven 3-DOF payload of Eq. (25) undergoes approximate linearization with the use of first-order Taylor series expansion and through the computation of the associated Jacobian matrices. The linearization process takes place at each sampling instance around the temporary operating point (x^*, u^*) where x^* is the present value of the system's state vector and u^* is the last sampled value of its control inputs vector (that is the tensions of the cables). The modelling error which is due to the truncation of higher-order terms from the Taylor series expansion is considered to be a perturbation which is asymptotically compensated by the robustness of the control method.

The initial nonlinear state-space model of the cable-suspended payload being in the form $\dot{x} = f(x) + g(x)u$, after linearization comes into the form:

$$\dot{x} = Ax + Bu + \tilde{d} \quad (59)$$

where matrices A , B are the Jacobian matrices of the system:

$$A = \nabla_x [f(x) + g(x)u] |_{(x^*, u^*)} \Rightarrow A = \nabla_x f(x) |_{(x^*, u^*)} + \nabla_x g_1(x)u_1 |_{(x^*, u^*)} + \nabla_x g_2(x)u_2 |_{(x^*, u^*)} \quad (60)$$

$$B = \nabla_u [f(x) + g(x)u] |_{(x^*, u^*)} \Rightarrow B = g(x) |_{(x^*, u^*)} \quad (61)$$

where the cumulative vector of disturbances (x^*, u^*) comprises (i) modelling error due to truncation of higher-order terms from the Taylor series expansion, (ii) external disturbances, (iii) sensor measurement noise of any distribution. Because of linearizing at each sampling instance around the present position of the crane's state vector, the span of the Taylor series expansion is small and the modelling error is negligible.

Next, the Jacobian matrix $\nabla_x f(x) |_{(x^*, u^*)}$ is computed.

First row of the Jacobian matrix $\nabla_x f(x) |_{(x^*, u^*)}$: $\frac{\partial f_1}{\partial x_1} = 0$, $\frac{\partial f_1}{\partial x_2} = 1$, $\frac{\partial f_1}{\partial x_3} = 0$, $\frac{\partial f_1}{\partial x_4} = 0$, $\frac{\partial f_1}{\partial x_5} = 0$ and $\frac{\partial f_1}{\partial x_6} = 0$.

Second row of the Jacobian matrix $\nabla_x f(x) |_{(x^*, u^*)}$: It holds that

$$f_2 = \frac{f_{2,num}}{f_{2,den}} = \frac{-M_{11}C_1 + M_{21}C_2 - M_{31}G_3}{detM} \quad (62)$$

It holds that for $1, 2, \dots, 6$

$$\frac{\partial f_2}{\partial x_i} = \frac{\frac{\partial f_{2,num}}{\partial x_i} detM - f_{2,num} \frac{\partial detM}{\partial x_i}}{detM^2} \quad (63)$$

where for $1, 2, \dots, 6$

$$\frac{\partial f_{2,num}}{\partial x_i} = -\frac{\partial M_{11}}{\partial x_i} C_1 - M_{11} \frac{\partial C_1}{\partial x_i} + \frac{\partial M_{21}}{\partial x_i} C_2 + M_{21} \frac{\partial C_2}{\partial x_i} - \frac{\partial M_{31}}{\partial x_i} G_3 - M_{31} \frac{\partial G_3}{\partial x_i} \quad (64)$$

and also for $1, 2, \dots, 6$

$$\frac{\partial detM}{\partial x_i} = (M + m) \frac{\partial M_{11}}{\partial x_i} - (mL_3 \sin(x_5)) M_{13} + mL_3 \cos(x_5) \frac{\partial M_{13}}{\partial x_i} \quad (65)$$

Third row of the Jacobian matrix $\nabla_x f(x) |_{(x^*, u^*)}$: $\frac{\partial f_3}{\partial x_1} = 0$, $\frac{\partial f_3}{\partial x_2} = 0$, $\frac{\partial f_3}{\partial x_3} = 0$, $\frac{\partial f_3}{\partial x_4} = 1$, $\frac{\partial f_3}{\partial x_5} = 0$ and $\frac{\partial f_3}{\partial x_6} = 0$.

Fourth row of the Jacobian matrix $\nabla_x f(x) |_{(x^*, u^*)}$: It holds that

$$f_4 = \frac{f_{4,num}}{f_{4,den}} = \frac{M_{12}C_1 - M_{22}C_2 + M_{32}G_3}{\det M} \quad (66)$$

It holds that for $1, 2, \dots, 6$

$$\frac{\partial f_4}{\partial x_i} = \frac{\frac{\partial f_{4,num}}{\partial x_i} \det M - f_{4,num} \frac{\partial \det M}{\partial x_i}}{\det M^2} \quad (67)$$

where for $1, 2, \dots, 6$

$$\frac{\partial f_{4,num}}{\partial x_i} = \frac{\partial M_{12}}{\partial x_i} C_1 + M_{12} \frac{\partial C_1}{\partial x_i} - \frac{\partial M_{22}}{\partial x_i} C_2 - M_{22} \frac{\partial C_2}{\partial x_i} + \frac{\partial M_{32}}{\partial x_i} G_3 + M_{32} \frac{\partial G_3}{\partial x_i} \quad (68)$$

Fifth row of the Jacobian matrix $\nabla_x f(x) |_{(x^*, u^*)}$: $\frac{\partial f_5}{\partial x_1} = 0$, $\frac{\partial f_5}{\partial x_2} = 0$, $\frac{\partial f_5}{\partial x_3} = 0$, $\frac{\partial f_5}{\partial x_4} = 0$, $\frac{\partial f_5}{\partial x_5} = 0$ and $\frac{\partial f_5}{\partial x_6} = 1$.

Sixth row of the Jacobian matrix $\nabla_x f(x) |_{(x^*, u^*)}$: It holds that

$$f_6 = \frac{f_{6,num}}{f_{6,den}} = \frac{-M_{13}C_1 + M_{23}C_2 - M_{33}G_3}{\det M} \quad (69)$$

It holds that for $1, 2, \dots, 6$

$$\frac{\partial f_6}{\partial x_i} = \frac{\frac{\partial f_{6,num}}{\partial x_i} \det M - f_{6,num} \frac{\partial \det M}{\partial x_i}}{\det M^2} \quad (70)$$

where for $1, 2, \dots, 6$

$$\frac{\partial f_{6,num}}{\partial x_i} = \frac{-\partial M_{13}}{\partial x_i} C_1 - M_{13} \frac{\partial C_1}{\partial x_i} + \frac{\partial M_{23}}{\partial x_i} C_2 + M_{23} \frac{\partial C_2}{\partial x_i} - \frac{\partial M_{33}}{\partial x_i} G_3 - M_{33} \frac{\partial G_3}{\partial x_i} \quad (71)$$

Next, the Jacobian matrix $\nabla_x g_1(x) |_{(x^*, u^*)}$ is computed.

First row of the Jacobian matrix $\nabla_x g_1(x) |_{(x^*, u^*)}$: $\frac{\partial g_{11}}{\partial x_i} = 0$. for $i = 1, 2, \dots, 6$.

Second row of the Jacobian matrix $\nabla_x g_1(x) |_{(x^*, u^*)}$: It holds that for $i = 1, 2, \dots, 6$

$$\frac{\partial g_{21}}{\partial x_i} = \frac{\frac{\partial M_{11}}{\partial x_i} \det M - M_{11} \frac{\partial \det M}{\partial x_i}}{\det M^2} \quad (72)$$

Third row of the Jacobian matrix $\nabla_x g_1(x) |_{(x^*, u^*)}$: $\frac{\partial g_{31}}{\partial x_i} = 0$. for $i = 1, 2, \dots, 6$.

Fourth row of the Jacobian matrix $\nabla_x g_1(x) |_{(x^*, u^*)}$: It holds that for $i = 1, 2, \dots, 6$

$$\frac{\partial g_{41}}{\partial x_i} = \frac{-\frac{\partial M_{12}}{\partial x_i} \det M + M_{12} \frac{\partial \det M}{\partial x_i}}{\det M^2} \quad (73)$$

Fifth row of the Jacobian matrix $\nabla_x g_1(x) |_{(x^*, u^*)}$: $\frac{\partial g_{51}}{\partial x_i} = 0$. for $i = 1, 2, \dots, 6$.

Sixth row of the Jacobian matrix $\nabla_x g_1(x) |_{(x^*, u^*)}$: It holds that for $i = 1, 2, \dots, 6$

$$\frac{\partial g_{61}}{\partial x_i} = \frac{\frac{\partial M_{13}}{\partial x_i} \det M - M_{13} \frac{\partial \det M}{\partial x_i}}{\det M^2} \quad (74)$$

Next, the Jacobian matrix $\nabla_x g_2(x) |_{(x^*, u^*)}$ is computed.

First row of the Jacobian matrix $\nabla_x g_2(x) |_{(x^*, u^*)}$: $\frac{\partial g_{12}}{\partial x_i} = 0$. for $i = 1, 2, \dots, 6$.

Second row of the Jacobian matrix $\nabla_x g_2(x) |_{(x^*, u^*)}$: It holds that for $i = 1, 2, \dots, 6$

$$\frac{\partial g_{22}}{\partial x_i} = \frac{-\frac{\partial M_{12}}{\partial x_i} \det M + M_{12} \frac{\partial \det M}{\partial x_i}}{\det M^2} \quad (75)$$

Third row of the Jacobian matrix $\nabla_x g_2(x) |_{(x^*, u^*)}$: $\frac{\partial g_{32}}{\partial x_i} = 0$. for $i = 1, 2, \dots, 6$.

Fourth row of the Jacobian matrix $\nabla_x g_2(x) |_{(x^*, u^*)}$: It holds that for $i = 1, 2, \dots, 6$

$$\frac{\partial g_{42}}{\partial x_i} = \frac{\frac{\partial M_{22}}{\partial x_i} \det M - M_{22} \frac{\partial \det M}{\partial x_i}}{\det M^2} \quad (76)$$

Fifth row of the Jacobian matrix $\nabla_x g_2(x) |_{(x^*, u^*)}$: $\frac{\partial g_{52}}{\partial x_i} = 0$. for $i = 1, 2, \dots, 6$.

Sixth row of the Jacobian matrix $\nabla_x g_2(x) |_{(x^*, u^*)}$: It holds that for $i = 1, 2, \dots, 6$

$$\frac{\partial g_{62}}{\partial x_i} = \frac{-\frac{\partial M_{32}}{\partial x_i} \det M + M_{32} \frac{\partial \det M}{\partial x_i}}{\det M^2} \quad (77)$$

Computation of the partial derivatives of the sub-determinants of the inertia matrix:

It holds that $\frac{\partial M_{11}}{\partial x_i} = 0$ for $i = 1, 2, \dots, 6$ and $i \neq 5$ while $\frac{\partial M_{11}}{\partial x_5} = -(ML_3)^2 \sin(x_5) \cos(x_5)$.

Additionally, it holds that $\frac{\partial M_{12}}{\partial x_i} = 0$ for $i = 1, 2, \dots, 6$ and $i \neq 5$ while $\frac{\partial M_{12}}{\partial x_5} = -(mL_3)^2 [\cos(x_5)^2 - \sin(x_5)^2]$.

Moreover, it holds that $\frac{\partial M_{13}}{\partial x_i} = 0$ for $i = 1, 2, \dots, 6$ and $i \neq 5$ while $\frac{\partial M_{13}}{\partial x_5} = (M + m)(mL_3) \sin(x_5)$.

Furthermore, one has that $\frac{\partial M_{21}}{\partial x_i} = 0$ for $i = 1, 2, \dots, 6$ and $i \neq 5$ while $\frac{\partial M_{21}}{\partial x_5} = -(mL_3)^2 [\cos(x_5)^2 - \sin(x_5)^2]$.

Additionally, it holds that $\frac{\partial M_{22}}{\partial x_i} = 0$ for $i = 1, 2, \dots, 6$ and $i \neq 5$ while $\frac{\partial M_{22}}{\partial x_5} = 2(mL_3)^2 \sin(x_5) \cos(x_5)$.

Moreover, it holds that $\frac{\partial M_{23}}{\partial x_i} = 0$ for $i = 1, 2, \dots, 6$ and $i \neq 5$ while $\frac{\partial M_{23}}{\partial x_5} = (M + m)(mL_3) \cos(x_5)$.

Furthermore, one has that $\frac{\partial M_{31}}{\partial x_i} = 0$ for $i = 1, 2, \dots, 6$ and $i \neq 5$ while $\frac{\partial M_{31}}{\partial x_5} = (M + m)(mL_3) \sin(x_5)$.

Moreover, it holds that $\frac{\partial M_{32}}{\partial x_i} = 0$ for $i = 1, 2, \dots, 6$ and $i \neq 5$ while $\frac{\partial M_{32}}{\partial x_5} = (M + m)(mL_3) \cos(x_5)$.

Finally, it holds that $\frac{\partial M_{33}}{\partial x_i} = 0$ for $i = 1, 2, \dots, 6$.

Computation of the partial derivatives of the non-zero elements of the Coriolis forces vector $C(q, \dot{q})$:

It holds that $\frac{\partial C_1}{\partial x_1} = 0$, $\frac{\partial C_1}{\partial x_2} = 0$, $\frac{\partial C_1}{\partial x_3} = 0$, $\frac{\partial C_1}{\partial x_4} = 0$, $\frac{\partial C_1}{\partial x_5} = -(mL_3 \cos(x_5))x_6^2$, and $\frac{\partial C_1}{\partial x_6} = -2(mL_3 \sin(x_5))x_6$.

Moreover, it holds that $\frac{\partial C_2}{\partial x_1} = 0$, $\frac{\partial C_2}{\partial x_2} = 0$, $\frac{\partial C_2}{\partial x_3} = 0$, $\frac{\partial C_2}{\partial x_4} = 0$, $\frac{\partial C_2}{\partial x_5} = -(mL_3 \sin(x_5))x_6^2$, and $\frac{\partial C_2}{\partial x_6} = 2(mL_3 \cos(x_5))x_6$.

Computation of the partial derivatives of the non-zero elements of the gravitational forces vector $G(q)$:

It holds that $\frac{\partial G_3}{\partial x_1} = 0$, $\frac{\partial G_3}{\partial x_2} = 0$, $\frac{\partial G_3}{\partial x_3} = 0$, $\frac{\partial G_3}{\partial x_4} = 0$, $\frac{\partial G_3}{\partial x_5} = (mgL_3 \cos(x_5))$, and $\frac{\partial G_3}{\partial x_6} = 0$.

Remark: It is noted that the linearization approach which has been followed for implementing the nonlinear optimal control scheme results into a quite accurate model of the system's dynamics. Consider for instance the following affine-in-the-input state-space model

$$\begin{aligned} \dot{x} &= f(x) + g(x)u \Rightarrow \\ \dot{x} &= [f(x^*) + \nabla_x f(x) |_{x^*} (x - x^*)] + [g(x^*) + \nabla_x g(x) |_{x^*} (x - x^*)]u^* + g(x^*)u^* + g(x^*)(u - u^*) + \tilde{d}_1 \Rightarrow \\ \dot{x} &= [\nabla_x f(x) |_{x^*} + \nabla_x g(x) |_{x^*} u^*]x + g(x^*)u - [\nabla_x f(x) |_{x^*} + \nabla_x g(x) |_{x^*} u^*]x^* + f(x^*) + g(x^*)u^* + \tilde{d}_1 \end{aligned} \quad (78)$$

where \tilde{d}_1 is the modelling error due to truncation of higher order terms in the Taylor series expansion of $f(x)$ and $g(x)$. Next, by defining $A = [\nabla_x f(x) |_{x^*} + \nabla_x g(x) |_{x^*} u^*]$, $B = g(x^*)$ one obtains

$$\dot{x} = Ax + Bu - Ax^* + f(x^*) + g(x^*)u^* + \tilde{d}_1 \quad (79)$$

Moreover by denoting $\tilde{d} = -Ax^* + f(x^*) + g(x^*)u^* + \tilde{d}_1$ about the cumulative modelling error term in the Taylor series expansion procedure one has

$$\dot{x} = Ax + Bu + \tilde{d} \quad (80)$$

which is the approximately linearized model of the dynamics of the system of Eq. (59). The term $f(x^*) + g(x^*)u^*$ is the derivative of the state vector at (x^*, u^*) which is almost annihilated by $-Ax^*$.

4.2 Equivalent linearized dynamics of the cable-driven payload

After linearization around its current operating point, the dynamic model for the two cable-driven 3-DOF payload is written as

$$\dot{x} = Ax + Bu + d_1 \quad (81)$$

Parameter d_1 stands for the linearization error in the two cable-driven 3-DOF payload's model that was given previously in Eq. (81). The reference setpoints for the state vector of the aforementioned dynamic model are denoted by $\mathbf{x}_d = [x_1^d, \dots, x_6^d]$. Tracking of this trajectory is achieved after applying the control input u^* . At every time instant the control input u^* is assumed to differ from the control input u appearing in Eq. (81) by an amount equal to Δu , that is $u^* = u + \Delta u$

$$\dot{x}_d = Ax_d + Bu^* + d_2 \quad (82)$$

The dynamics of the controlled system described in Eq. (81) can be also written as

$$\dot{x} = Ax + Bu + Bu^* - Bu^* + d_1 \quad (83)$$

and by denoting $d_3 = -Bu^* + d_1$ as an aggregate disturbance term one obtains

$$\dot{x} = Ax + Bu + Bu^* + d_3 \quad (84)$$

By subtracting Eq. (82) from Eq. (84) one has

$$\dot{x} - \dot{x}_d = A(x - x_d) + Bu + d_3 - d_2 \quad (85)$$

By denoting the tracking error as $e = x - x_d$ and the aggregate disturbance term as $L\tilde{d} = d_3 - d_2$, the tracking error dynamics becomes

$$\dot{e} = Ae + Bu + L\tilde{d} \quad (86)$$

where L is a disturbance inputs gain matrix. The above linearized form of the two cable-driven 3-DOF payload's model can be efficiently controlled after applying an H-infinity feedback control scheme.

4.3 The nonlinear H-infinity control

The initial nonlinear model of the two cable-driven 3-DOF payload is in the form

$$\dot{x} = f(x, u) \quad x \in R^n, \quad u \in R^m \quad (87)$$

Linearization of the model of the two cable-driven 3-DOF payload is performed at each iteration of the control algorithm around its present operating point $(x^*, u^*) = (x(t), u(t - T_s))$. The linearized equivalent of the system is described by

$$\dot{x} = Ax + Bu + L\tilde{d} \quad x \in R^n, \quad u \in R^m, \quad \tilde{d} \in R^q \quad (88)$$

where matrices A and B are obtained from the computation of the previously defined Jacobians and vector \tilde{d} denotes disturbance terms due to linearization errors, while L is a disturbance inputs gain matrix. The problem of disturbance rejection for the linearized model that is described by

$$\begin{aligned} \dot{x} &= Ax + Bu + L\tilde{d} \\ y &= Cx \end{aligned} \quad (89)$$

where $x \in R^n$, $u \in R^m$, $\tilde{d} \in R^q$ and $y \in R^p$, cannot be handled efficiently if the classical LQR control scheme is applied. This is because of the existence of the perturbation term \tilde{d} . The disturbance term \tilde{d} apart from modeling (parametric) uncertainty and external perturbations can also represent noise terms of any distribution.

In the H_∞ control approach, a feedback control scheme is designed for trajectory tracking by the system's state vector and simultaneous disturbance rejection, considering that the disturbance affects the system in the worst possible manner. The disturbances' effects are incorporated in the following quadratic cost function:

$$J(t) = \frac{1}{2} \int_0^T [y^T(t)y(t) + ru^T(t)u(t) - \rho^2 \tilde{d}^T(t)\tilde{d}(t)]dt, \quad r, \rho > 0 \quad (90)$$

The significance of the negative sign in the cost function's term that is associated with the perturbation variable $\tilde{d}(t)$ is that the disturbance tries to maximize the cost function $J(t)$ while the control signal $u(t)$ tries to minimize it. The physical meaning of the relation given above is that the control signal and the disturbances compete to each other within a min-max differential game. This problem of min-max optimization can be written as $\min_u \max_{\tilde{d}} J(u, \tilde{d})$.

The objective of the optimization procedure is to compute a control signal $u(t)$ which can compensate for the worst possible disturbance, that is externally imposed to the two cable-driven 3-DOF payload. However, the solution to the min-max optimization problem is directly related to the value of parameter ρ . This means that there is an upper bound in the disturbances magnitude that can be annihilated by the control signal.

4.4 Computation of the feedback control gains

For the linearized system given by Eq. (89) the cost function of Eq. (90) is defined, where coefficient r determines the penalization of the control input and weight coefficient ρ determines the reward of the disturbances' effects. It is assumed that (i) The energy that is transferred from the disturbances signal $\tilde{d}(t)$ is bounded, that is $\int_0^\infty \tilde{d}^T(t)\tilde{d}(t)dt < \infty$, (ii) matrices $[A, B]$ and $[A, L]$ are stabilizable, (iii) matrix $[A, C]$ is detectable. In the case of a tracking problem the optimal feedback control law is given by

$$u(t) = -Ke(t) \quad (91)$$

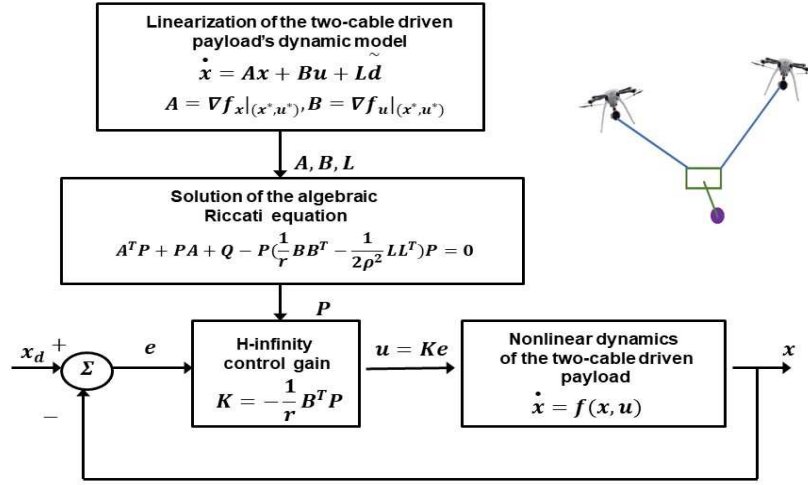


Figure 3: Control scheme and implementation stages for the two cable-driven 3-DOF payload

with $e = x - x_d$ to be the tracking error, and $K = \frac{1}{r} B^T P$ where P is a positive definite symmetric matrix. As it will be proven in Section 4, matrix P is obtained from the solution of the Riccati equation

$$A^T P + PA + Q - P(\frac{2}{r} BB^T - \frac{1}{\rho^2} LL^T)P = 0 \quad (92)$$

where Q is a positive semi-definite symmetric matrix. The worst case disturbance is given by

$$\tilde{d}(t) = \frac{1}{\rho^2} L^T P e(t) \quad (93)$$

The solution of the H-infinity feedback control problem for the two cable-driven 3-DOF payload and the computation of the worst case disturbance that the related controller can sustain, comes from superposition of Bellman's optimality principle when considering that the two cable-driven 3-DOF payload is affected by two separate inputs (i) the control input u (ii) the cumulative disturbance input $\tilde{d}(t)$. Solving the optimal control problem for u , that is for the minimum variation (optimal) control input that achieves elimination of the state vector's tracking error, gives $u = -\frac{1}{r} B^T P e$. Equivalently, solving the optimal control problem for \tilde{d} , that is for the worst case disturbance that the control loop can sustain gives $\tilde{d} = \frac{1}{\rho^2} L^T P e$.

The diagram of the considered control loop for the two cable-driven payload is depicted in Fig. 3.

4.5 Stability proof for the optimally controlled payload

Through Lyapunov stability analysis it will be shown that the proposed nonlinear control scheme assures H_∞ tracking performance for the two cable-driven 3-DOF payload, and that in case of bounded disturbance terms asymptotic convergence to the reference setpoints is achieved. The tracking error dynamics for the two cable-driven 3-DOF payload is written in the form

$$\dot{e} = Ae + Bu + L\tilde{d} \quad (94)$$

where in the two cable-driven 3-DOF payload's case $L = \in R^{6 \times 6}$ is the disturbance inputs gain matrix. Variable \tilde{d} denotes model uncertainties and external disturbances of the two cable-driven 3-DOF payload's model. The following Lyapunov equation is considered

$$V = \frac{1}{2}e^T P e \quad (95)$$

where $e = x - x_d$ is the tracking error. By differentiating with respect to time one obtains

$$\begin{aligned} \dot{V} &= \frac{1}{2}\dot{e}^T P e + \frac{1}{2}e^T P \dot{e} \Rightarrow \\ \dot{V} &= \frac{1}{2}[Ae + Bu + L\tilde{d}]^T P e + \frac{1}{2}e^T P [Ae + Bu + L\tilde{d}] \Rightarrow \end{aligned} \quad (96)$$

$$\begin{aligned} \dot{V} &= \frac{1}{2}[e^T A^T + u^T B^T + \tilde{d}^T L^T] P e + \\ &+ \frac{1}{2}e^T P [Ae + Bu + L\tilde{d}] \Rightarrow \end{aligned} \quad (97)$$

$$\begin{aligned} \dot{V} &= \frac{1}{2}e^T A^T P e + \frac{1}{2}u^T B^T P e + \frac{1}{2}\tilde{d}^T L^T P e + \\ &\frac{1}{2}e^T P A e + \frac{1}{2}e^T P B u + \frac{1}{2}e^T P L \tilde{d} \end{aligned} \quad (98)$$

The previous equation is rewritten as

$$\begin{aligned} \dot{V} &= \frac{1}{2}e^T (A^T P + P A) e + (\frac{1}{2}u^T B^T P e + \frac{1}{2}e^T P B u) + \\ &+ (\frac{1}{2}\tilde{d}^T L^T P e + \frac{1}{2}e^T P L \tilde{d}) \end{aligned} \quad (99)$$

Assumption: For given positive definite matrix Q and coefficients r and ρ there exists a positive definite matrix P , which is the solution of the following matrix equation

$$A^T P + P A = -Q + P(\frac{2}{r}BB^T - \frac{1}{\rho^2}LL^T)P \quad (100)$$

Moreover, the following feedback control law is applied to the system

$$u = -\frac{1}{r}B^T P e \quad (101)$$

By substituting Eq. (100) and Eq. (101) one obtains

$$\begin{aligned} \dot{V} &= \frac{1}{2}e^T [-Q + P(\frac{2}{r}BB^T - \frac{1}{\rho^2}LL^T)P] e + \\ &+ e^T P B (-\frac{1}{r}B^T P e) + e^T P L \tilde{d} \Rightarrow \end{aligned} \quad (102)$$

$$\begin{aligned} \dot{V} &= -\frac{1}{2}e^T Q e + \frac{1}{r}e^T P B B^T P e - \frac{1}{2\rho^2}e^T P L L^T P e \\ &- \frac{1}{r}e^T P B B^T P e + e^T P L \tilde{d} \end{aligned} \quad (103)$$

which after intermediate operations gives

$$\dot{V} = -\frac{1}{2}e^T Q e - \frac{1}{2\rho^2}e^T P L L^T P e + e^T P L \tilde{d} \quad (104)$$

or, equivalently

$$\begin{aligned} \dot{V} &= -\frac{1}{2}e^T Q e - \frac{1}{2\rho^2}e^T P L L^T P e + \\ &+ \frac{1}{2}e^T P L \tilde{d} + \frac{1}{2}\tilde{d}^T L^T P e \end{aligned} \quad (105)$$

Lemma: The following inequality holds

$$\frac{1}{2}e^T L \tilde{d} + \frac{1}{2}\tilde{d}^T L^T P e - \frac{1}{2\rho^2}e^T P L L^T P e \leq \frac{1}{2}\rho^2 \tilde{d}^T \tilde{d} \quad (106)$$

Proof: The binomial $(\rho\alpha - \frac{1}{\rho}b)^2$ is considered. Expanding the left part of the above inequality one gets

$$\begin{aligned} \rho^2 a^2 + \frac{1}{\rho^2} b^2 - 2ab &\geq 0 \Rightarrow \frac{1}{2}\rho^2 a^2 + \frac{1}{2\rho^2} b^2 - ab \geq 0 \Rightarrow \\ ab - \frac{1}{2\rho^2} b^2 &\leq \frac{1}{2}\rho^2 a^2 \Rightarrow \frac{1}{2}ab + \frac{1}{2}ab - \frac{1}{2\rho^2} b^2 \leq \frac{1}{2}\rho^2 a^2 \end{aligned} \quad (107)$$

The following substitutions are carried out: $a = \tilde{d}$ and $b = e^T PL$ and the previous relation becomes

$$\frac{1}{2}\tilde{d}^T L^T P e + \frac{1}{2}e^T P L \tilde{d} - \frac{1}{2\rho^2}e^T P L L^T P e \leq \frac{1}{2}\rho^2 \tilde{d}^T \tilde{d} \quad (108)$$

Eq. (108) is substituted in Eq. (105) and the inequality is enforced, thus giving

$$\dot{V} \leq -\frac{1}{2}e^T Q e + \frac{1}{2}\rho^2 \tilde{d}^T \tilde{d} \quad (109)$$

Eq. (109) shows that the H_∞ tracking performance criterion is satisfied. The integration of \dot{V} from 0 to T gives

$$\begin{aligned} \int_0^T \dot{V}(t) dt &\leq -\frac{1}{2} \int_0^T \|e\|_Q^2 dt + \frac{1}{2}\rho^2 \int_0^T \|\tilde{d}\|^2 dt \Rightarrow \\ 2V(T) + \int_0^T \|e\|_Q^2 dt &\leq 2V(0) + \rho^2 \int_0^T \|\tilde{d}\|^2 dt \end{aligned} \quad (110)$$

Moreover, if there exists a positive constant $M_d > 0$ such that

$$\int_0^\infty \|\tilde{d}\|^2 dt \leq M_d \quad (111)$$

then one gets

$$\int_0^\infty \|e\|_Q^2 dt \leq 2V(0) + \rho^2 M_d \quad (112)$$

Thus, the integral $\int_0^\infty \|e\|_Q^2 dt$ is bounded. Moreover, $V(T)$ is bounded and from the definition of the Lyapunov function V in Eq. (95) it becomes clear that $e(t)$ will be also bounded since $e(t) \in \Omega_e = \{e | e^T P e \leq 2V(0) + \rho^2 M_d\}$. According to the above and with the use of Barbalat's Lemma one obtains $\lim_{t \rightarrow \infty} e(t) = 0$.

After following the stages of the stability proof one arrives at Eq. (109) which shows that the H-infinity tracking performance criterion holds. By selecting the attenuation coefficient ρ to be sufficiently small and in particular to satisfy $\rho^2 < \|e\|_Q^2 / \|\tilde{d}\|^2$ one has that the first derivative of the Lyapunov function is upper bounded by 0. This condition holds at each sampling instance and consequently global stability for the control loop can be concluded.

5 Flatness-based control in successive loops for the quadrotors

It will be proven that each one of the subsystems of Eq. (55) and Eq. (56) of the dynamic model of the quadrotors is differentially flat, and that stabilizing feedback control about them can be achieved by applying a dynamics inversion technique which is commonly used in input-output linearized systems.

For the subsystem of Eq. (55) the flat outputs vector is taken to be $Y_1 = x_{1,6}$ while $x_{7,12}$ is taken to be a virtual control input, that is $\bar{v}_1 = x_{7,12}$. Thus, solving Eq. (55) for \bar{v}_1 one obtains Eq. (57) which signifies that \bar{v}_1 is a differential function of the flat outputs Y_1 . Consequently, Eq. (55) is a differentially flat subsystem.

For the subsystem of Eq. (56) the flat outputs vector is taken to be $Y_2 = x_{7,12}$ while $x_{1,6}$ is taken to be a coefficients vector and u is the real control input. Thus, solving Eq. (56) for u one obtains Eq. (58) which signifies that u is a differential function of the flat outputs Y_2 . Consequently, Eq. (56) is a differentially flat subsystem.

In confirmation of the differential flatness properties of the subsystems of Eq. (55) and Eq. (56) one can notice that these subsystems are in the input-output linearized form. Consequently, control and stabilization about them can be achieved by applying common dynamics inversion techniques which have been used

for input-output linearized systems.

The setpoint for the subsystem of Eq. (55) is $x_{1,6}^*$ and the stabilizing feedback control is taken to be

$$\bar{v}_1 = x_{7,12}^* = g_{1,6}(x_{1,6})^{-1}[x_{1,6}^* - f(x_{1,6}) - K_1(x_{1,6} - x_{1,6}^*)] \quad (113)$$

where K_1 is a diagonal matrix $K_1 \in R^{6 \times 6}$ with diagonal elements $K_{1,ii} > 0$, $i = 1, 2, \dots, 6$. For the subsystem of Eq. (56) the stabilizing feedback control is taken to be

$$u = g_{7,12}(x_{1,6}, x_{7,12})^{-1}[x_{7,12}^* - f_{7,12}(x_{1,6}, x_{7,12}) - K_2(x_{7,12} - x_{7,12}^*)] \quad (114)$$

where K_2 is a diagonal matrix $K_2 \in R^{6 \times 6}$ with diagonal elements $K_{2,ii} > 0$, $i = 1, 2, \dots, 6$.

By applying the control law of Eq. (113) into the subsystem of Eq. (55) and by defining the tracking error variable $e_{1,6} = x_{1,6} - x_{1,6}^*$ one obtains

$$\begin{aligned} \dot{x}_{1,6} &= f_{1,6}(x_{1,3}) + g_{1,6}(x_{1,6})g_{1,6}(x_{1,6})^{-1}[x_{1,6}^* - f(x_{1,6}) - K_1(x_{1,6} - x_{1,6}^*)] \Rightarrow \\ &(\dot{x}_{1,6} - \dot{x}_{1,6}^*) + K_1(x_{1,6} - x_{1,6}^*) = 0 \Rightarrow \dot{e}_{1,6} + K_1 e_{1,6} = 0 \Rightarrow \\ &\lim_{t \rightarrow \infty} e_{1,6}(t) = 0 \Rightarrow \lim_{t \rightarrow \infty} x_{1,6}(t) = x_{1,6}^* \end{aligned} \quad (115)$$

By applying the control law of Eq. (114) into the subsystem of Eq. (56) and by defining the tracking error variable $e_{7,12} = x_{7,12} - x_{7,12}^*$ one obtains

$$\begin{aligned} \dot{x}_{7,12} &= f_{7,12}(x_{1,6}, x_{7,12}) + g_{7,12}(x_{1,6}, x_{7,12})g_{7,12}(x_{1,6}, x_{7,12})^{-1}[x_{7,12}^* - f(x_{7,12}) - K_2(x_{7,12} - x_{7,12}^*)] \Rightarrow \\ &(\dot{x}_{7,12} - \dot{x}_{7,12}^*) + K_2(x_{7,12} - x_{7,12}^*) = 0 \Rightarrow \dot{e}_{7,12} + K_2 e_{7,12} = 0 \Rightarrow \\ &\lim_{t \rightarrow \infty} e_{7,12}(t) = 0 \Rightarrow \lim_{t \rightarrow \infty} x_{7,12}(t) = x_{7,12}^* \end{aligned} \quad (116)$$

The global stability properties of the control method can be also proven through Lyapunov analysis. To this end, the following Lyapunov function is defined

$$V = \frac{1}{2}[e_{1,6}^T e_{1,6} + e_{7,12}^T e_{7,12}] \quad (117)$$

It holds that $V > 0 \forall e_{1,6} \neq 0, e_{7,12} \neq 0$ and $V = 0$ iff $e_{1,6} = 0, e_{7,12} = 0$. By differentiating in time the Lyapunov function of Eq. (117) one obtains

$$\dot{V} = \frac{1}{2}[2e_{1,6}^T \dot{e}_{1,6} + 2e_{7,12}^T \dot{e}_{7,12}] \quad (118)$$

Moreover, by using the tracking error dynamics of Eq. (115) and Eq. (116) one obtains

$$\begin{aligned} \dot{V} &= [e_{1,6}^T(-K_2 e_{1,6}) + e_{7,12}^T(-K_2 e_{7,12})] \Rightarrow \\ \dot{V} &= -e_{1,6}^T K_1 e_{1,6} - e_{7,12}^T K_2 e_{7,12} \Rightarrow \\ \dot{V} &< 0 \forall e_{1,6} \neq 0, e_{7,12} \neq 0 \end{aligned} \quad (119)$$

Therefore, V is a strictly diminishing function which converges asymptotically to 0. Consequently, it holds that $\lim_{t \rightarrow \infty} e_{1,6} = 0$ and $\lim_{t \rightarrow \infty} e_{7,12} = 0$.

An explicit demonstration of the exponential stabilization that is achieved by flatness-based control in successive loops is given next. The Lyapunov function of the control loop is written as:

$$V = \frac{1}{2}[\sum_{i=1}^6 e_i^2 + \sum_{j=7}^{12} e_j^2] \quad (120)$$

where e_i $i = 1, \dots, 6$ are the tracking errors for the state variables of the quadrotor associated with translational motion and e_j $j = 7, \dots, 12$ are the tracking errors for the state variables of the quadrotor

associated with rotational motion. Equivalently, the first-order time-derivative of the Lyapunov function is written as

$$\dot{V} = -[\sum_{i=1}^6 k_{1,i} e_i^2 + \sum_{j=7}^{12} k_{2,j} e_j^2] \quad (121)$$

where $k_{1,i} > 0$ $i = 1, \dots, 6$ are the diagonal elements of gain matrix K_1 and $k_{2,j} > 0$ $j = 7, \dots, 12$ are the diagonal elements of gain matrix K_2 . By denoting the minimum of the above-noted elements of the feedback gain matrices as k_{min} , that is

$$k_{min} = \min\{k_{1,i} : i = 1, \dots, 6 \text{ and } k_{2,j} : j = 7, \dots, 12\} \quad (122)$$

and using Eq. (121) one obtains that

$$\begin{aligned} \dot{V} &\leq -k_{min}[\sum_{i=1}^6 e_i^2 + \sum_{j=7}^{12} e_j^2] \\ \Rightarrow \dot{V} &\leq -2k_{min}V \Rightarrow \dot{V} + 2k_{min}V \leq 0 \end{aligned} \quad (123)$$

From Eq. (123) one can demonstrate the exponential convergence of the Lyapunov function V to 0.

The feedback control scheme, which is followed for the cascading subsystems that constitute the dynamic model of 6-DOF quadrotor and which is based on inversion of the subsystems' dynamics of this aerial drone, is equally robust to sliding-mode control in which the switching control term has been substituted by a saturation function. One can easily confirm this for the first-order i -th subsystem of the form $\dot{x}_i = f_i(x_i) + g_i(x_i)v_i$ by defining the sliding surface $s_i = e_i = x_i - x_i^d$ and the associated sliding mode controller $v_i = \hat{g}_i(x)^{-1}[\dot{x}_i^d - \hat{f}_i(x_i) - K_i \text{sgn}(x_i - x_i^d)]$ which after substituting the $\text{sgn}(s_i)$ function with the saturation $\text{sat}(s_i)$ function becomes $v_i = \hat{g}_i(x)^{-1}[\dot{x}_i^d - \hat{f}_i(x_i) - K_i(x_i - x_i^d)]$. The latter relation coincides with the flatness-based control in successive loops for the i -th subsystem under uncertainty (with use of the estimated functions $\hat{f}_i(x)$ and $\hat{g}_i(x)$) which is computed by the article's control method. Therefore, the proposed flatness-based control method in successive loops provides sufficient robustness margins which enable the reliable and safe functioning of each one of the two 6-DOF quadrotor under reasonable levels of model uncertainty or external perturbations.

6 Simulation tests

The simulation code was developed based on functional programming principles. There was a *main()* function which was executing sequentially inside a for-loop and at each sampling instance three other functions, namely (i) function *payload_transport()* which was performing the computation of the optimal control inputs for the transportation of the payload, (ii) function *quadrotor_UAV1()* which was performing control of the first UAV so as to achieve precise flight-path following and compensation of the force F_1 at the first cable, (iii) function *quadrotor_UAV2()* which was performing control of the second UAV so as to achieve precise flight-path following and compensation of the force F_2 at the second cable. The sampling period was $T_s = 0.01$ sec. To solve the algebraic Riccati equation of Eq. (100) so as to compute the optimal control inputs (lift forces) for the payload Matlab's function *aresolv()* was being executed at each sampling period.

Indicative values about the parameters of the payload's model have been: $M = 10.0\text{kg}$, $m = 20.0\text{kg}$, $L_1 = 2.5\text{m}$, $L_2 = 3.5\text{m}$, $L_3 = 1.0\text{m}$ and $g = 10\text{m/sec}^2$. Indicative values about the parameters of the 6-DOF quadrotor UAVs which have been used in the simulation experiments are given below: $m = 40\text{kg}$, $g = 10\text{m/sec}^2$, $K_x = 1.1$, $K_y = 1.1$, $K_z = 1.1$, $I_{xx} = 10.6\text{kg}\cdot\text{m}^2$, $I_{yy} = 10.6\text{kg}\cdot\text{m}^2$, $I_{zz} = 10.6\text{kg}\cdot\text{m}^2$, $I_{xy} = 0.6\text{kg}\cdot\text{m}^2$, $I_{xz} = 0.6\text{kg}\cdot\text{m}^2$, $I_{yz} = 0.6\text{kg}\cdot\text{m}^2$. The obtained results are depicted in Fig. 4 to Fig. 35. It can be noticed that in all test cases the proposed nonlinear optimal and multi-loop flatness-based control method achieved fast and accurate tracking of the reference setpoints, for both the payload and the two quadrotors, under moderate variations of the control inputs. Therefore, it can be concluded that

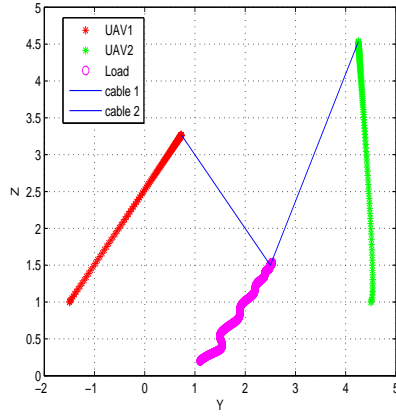
the proposed control scheme ensures safe transportation and precise final positioning of the payload at any point in the drones' operating space. The quadrotors may have different dynamic models while the lengths of the cables may also be uneven.

Regarding the implementation of the nonlinear optimal control for the cable-driven payload, the main parameters which affect the steady-state and the transient performance of this control scheme are the coefficients r , ρ and Q of the method's algebraic Riccati equation. For relatively small values of r the state vector's tracking error is eliminated. For relatively large values of the diagonal elements of matrix Q the speed of convergence to setpoints is increased. Finally, the smallest value of ρ for which one obtains a valid solution of the method's Riccati equation is the one that provides the control loop with maximum robustness. Unlike Nonlinear Model Predictive Control (NMPC) the global stability properties are proven and the convergence of the iterative search for the optimum of the new nonlinear optimal control method does not depend on initialization and ad-hoc selection of the controller's parameters. The nonlinear optimal control method minimizes the energy which is spent by the dual UAV transportation system for moving the load to its final position. The method is particularly suitable for underactuated systems such as the suspended payload, where the control inputs gain matrix is not in quadratic form and is not invertible.

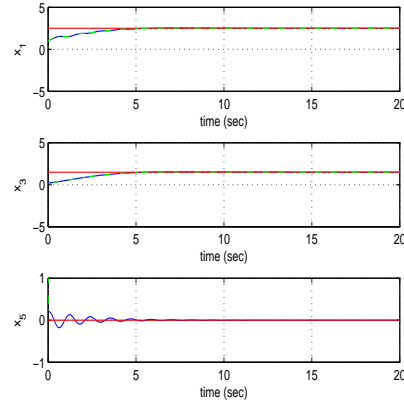
Regarding the implementation of multi-loop flatness-based it can be noticed again, that under this control scheme one achieves fast and precise tracking of reference setpoints for all state variables of the dynamic model of the 6-DOF autonomous quadrotor. It is noteworthy, that through the stages of this method one solves also the setpoints definition problem for all state variables of the quadrotor. Actually, the selection of setpoints for state variables x_4 to x_6 , that is $x_{4,6}^* = [\phi^*, \theta^*, \psi^*]^T$ is unconstrained. Regarding the selection of setpoints for state variables x_1 to x_3 , that is $x_{1,3}^* = [x^*, y^*, z^*]$, x^* is assigned a constant value because the drones move on the yz plane, and y^* , z^* for each drone satisfy the geometric constraints $y^* = y_{R,d} + L_i \cos(a_{i,d})$, $z^* = z_{R,d} + L_i \cos(a_{i,d})$ where L_i is the length of the cable and $a_{i,d}$ is the desirable angle between the OY axis and the cable. On the other side by defining state variables x_7 to x_{12} as virtual control inputs for the subsystem of state variables x_1 to x_6 one can find the setpoints for x_7 to x_{12} , denoted as $x_{7,12}^*$ as functions of the setpoints for x_1 to x_6 . The speed of convergence of the state variables of the 6-DOF autonomous quadrotor when using flatness-based control implemented in successive loops is determined by the selection of values for the diagonal gain matrices $K_1 \in R^{6 \times 6}$, $K_2 \in R^{6 \times 6}$.

7 Conclusions

The article has proposed a joint nonlinear optimal control and multi-loop flatness-based control approach for the control problem of the dual UAV cooperative load transportation. This dynamical system consisted of a cart with a payload suspended from it being driven by two cables which in turn were pulled by two quadrotors. The objective was to lift and transfer the payload to any desirable final position through suitable selection of the control inputs of the two UAVs. To secure the transportation process, the payload had to be stabilized at the vertical position while its oscillations around the vertical axis had to be rapidly and effectively suppressed. The control problem was of high difficulty because of involving different multi-DOF nonlinear dynamical systems, that is the cable-driven payload and the two drones, which were all underactuated. First, to compute the cables' forces which could stabilize the payload and could also ensure its safe transfer to the targeted final position, the associated nonlinear optimal control problem was solved. The dynamic model of the cable-suspended payload underwent an approximate linearization procedure through first-order Taylor series expansion and through the computation of the associated Jacobian matrices. The linearization was repeated at each sampling instance around a temporary operating point which was defined by the present value of the state vector of the cable-driven payload and by the last sampled value of the forces (tensions) of the cables which acted as control inputs to the payload. For the approximately linearized model of the cable-suspended payload an H-infinity controller was designed. To select the stabilizing feedback gains of the H-infinity controller an algebraic Riccati equation had to

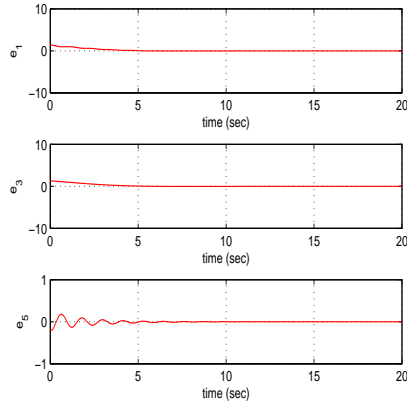


(a)

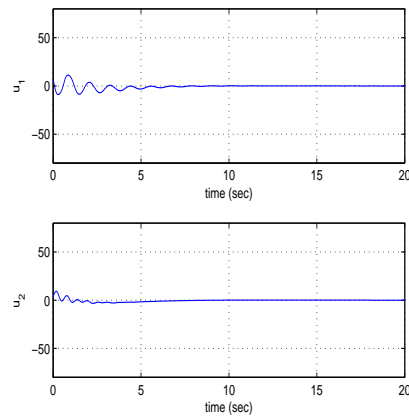


(b)

Figure 4: Tracking of setpoint 1 by the payload (a) trajectories in the OYZ plane followed by quadrotor 1 (red line) and quadrotor 2 (green line) and path followed by the cable-suspended payload (magenta line), (b) convergence of the state variables of the cable-suspended payload x_1 , x_3 and x_5 to the associated setpoints

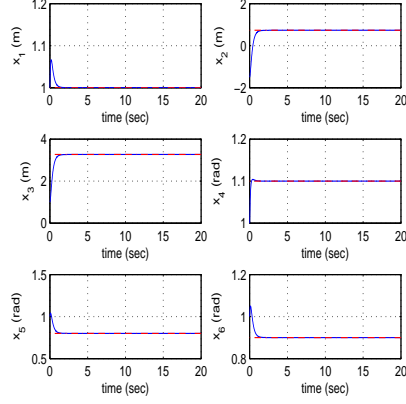


(a)

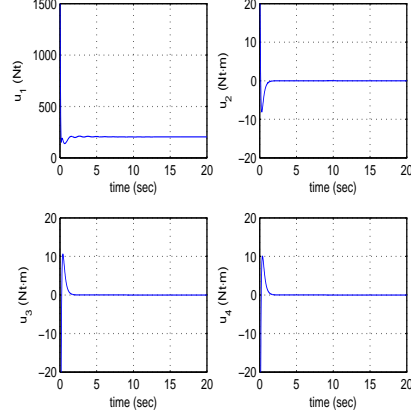


(b)

Figure 5: Tracking of setpoint 1 by the payload: (a) convergence to zero of the tracking error of state variables x_1 , x_3 and x_5 of the cable-suspended payload (b) variation of control inputs u_1 , u_2 applied to the payload through the cables

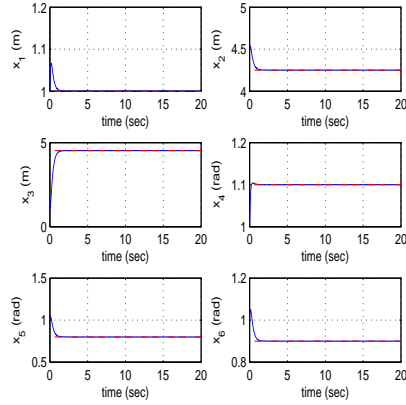


(a)

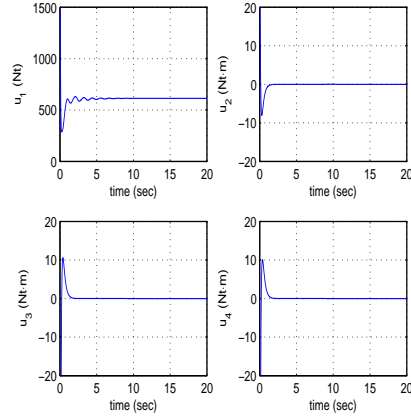


(b)

Figure 6: Tracking of setpoint 1 by the first UAV (a) convergence to setpoints (red line) for the state variables x_1 to x_6 of quadrotor 1 (blue line), (b) control inputs u_1 to u_4 of quadrotor 1 (blue line)

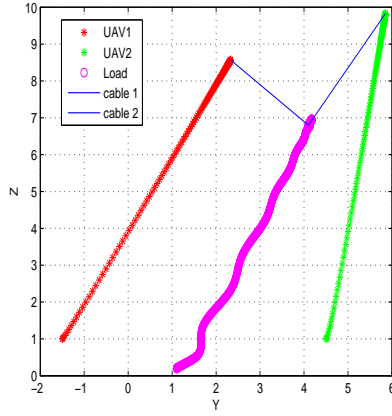


(a)

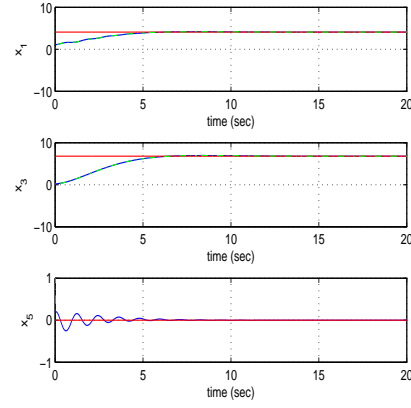


(b)

Figure 7: Tracking of setpoint 1 by the second UAV (a) convergence to setpoints (red line) for the state variables x_1 to x_6 of quadrotor 2 (blue line), (b) control inputs u_1 to u_4 of quadrotor 2 (blue line)

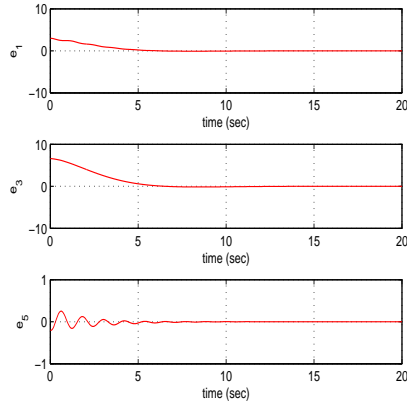


(a)

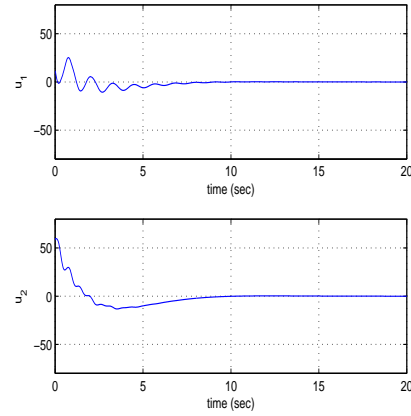


(b)

Figure 8: Tracking of setpoint 2 by the payload (a) trajectories in the OYZ plane followed by quadrotor 1 (red line) and quadrotor 2 (green line) and path followed by the cable-suspended payload (magenta line), (b) convergence of the state variables of the cable-suspended payload x_1 , x_3 and x_5 to the associated setpoints



(a)



(b)

Figure 9: Tracking of setpoint 2 by the payload: (a) convergence to zero of the tracking error of state variables x_1 , x_3 and x_5 of the cable-suspended payload (b) variation of control inputs u_1 , u_2 applied to the payload through the cables

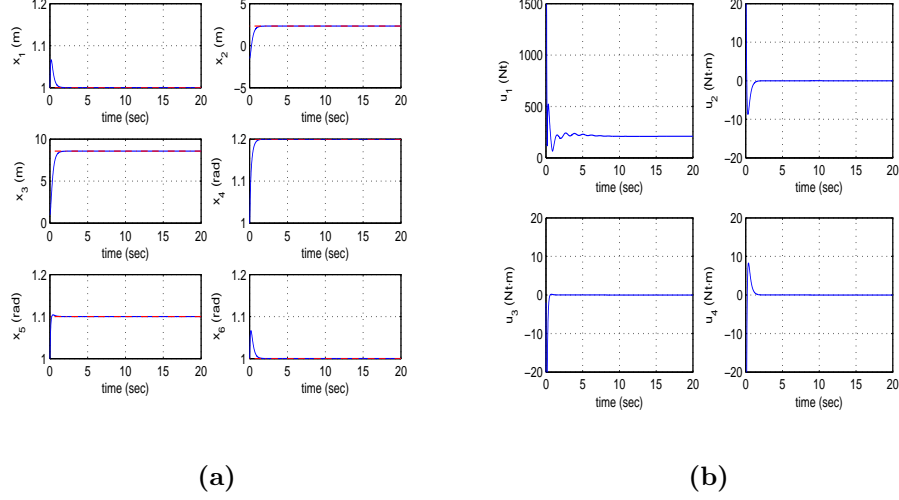


Figure 10: Tracking of setpoint 2 by the first UAV (a) convergence to setpoints (red line) for the state variables x_1 to x_6 of quadrotor 1 (blue line), (b) control inputs u_1 to u_4 of quadrotor 1 (blue line)

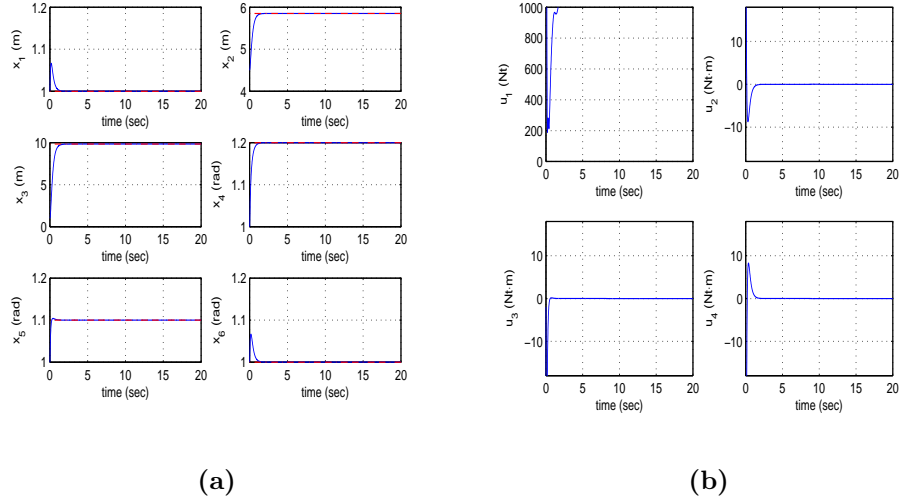
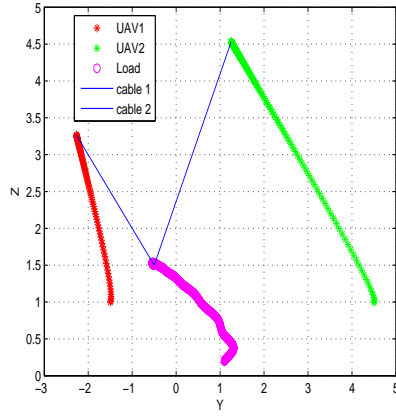
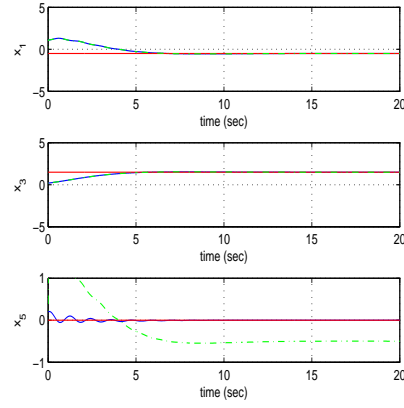


Figure 11: Tracking of setpoint 2 by the second UAV (a) convergence to setpoints (red line) for the state variables x_1 to x_6 of quadrotor 2 (blue line), (b) control inputs u_1 to u_4 of quadrotor 2 (blue line)

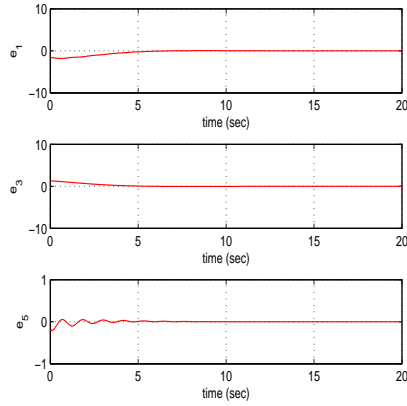


(a)

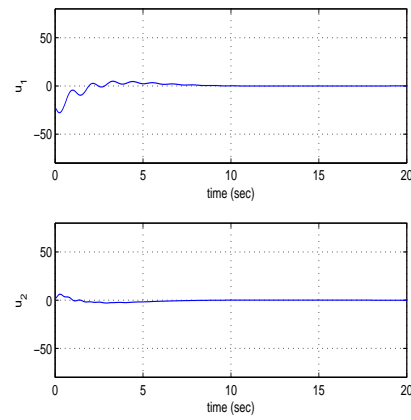


(b)

Figure 12: Tracking of setpoint 3 by the payload (a) trajectories in the OYZ plane followed by quadrotor 1 (red line) and quadrotor 2 (green line) and path followed by the cable-suspended payload (magenta line), (b) convergence of the state variables of the cable-suspended payload x_1 , x_3 and x_5 to the associated setpoints



(a)



(b)

Figure 13: Tracking of setpoint 3 by the payload: (a) convergence to zero of the tracking error of state variables x_1 , x_3 and x_5 of the cable-suspended payload (b) variation of control inputs u_1 , u_2 applied to the payload through the cables

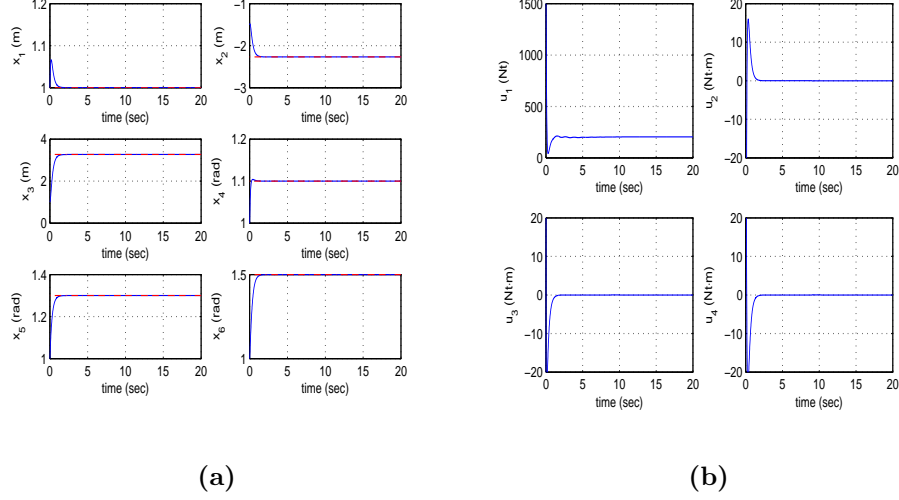


Figure 14: Tracking of setpoint 3 by the first UAV (a) convergence to setpoints (red line) for the state variables x_1 to x_6 of quadrotor 1 (blue line), (b) control inputs u_1 to u_4 of quadrotor 1 (blue line)

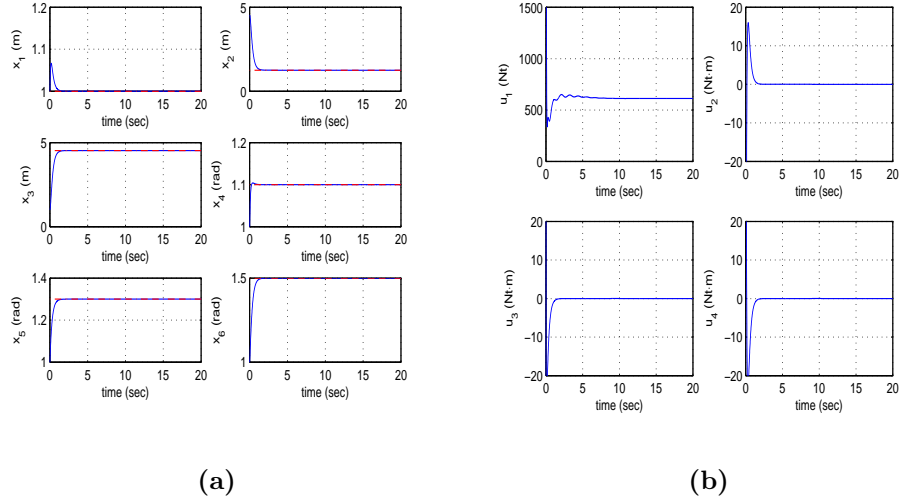
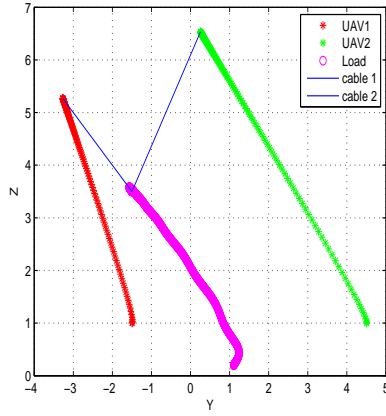
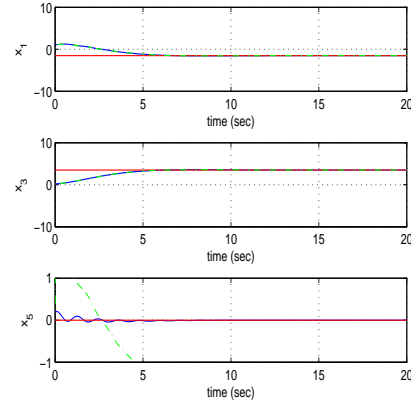


Figure 15: Tracking of setpoint 3 by the second UAV (a) convergence to setpoints (red line) for the state variables x_1 to x_6 of quadrotor 2 (blue line), (b) control inputs u_1 to u_4 of quadrotor 2 (blue line)

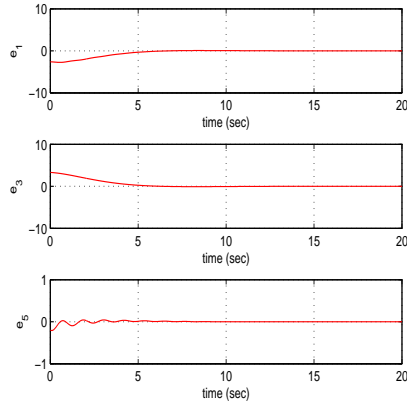


(a)

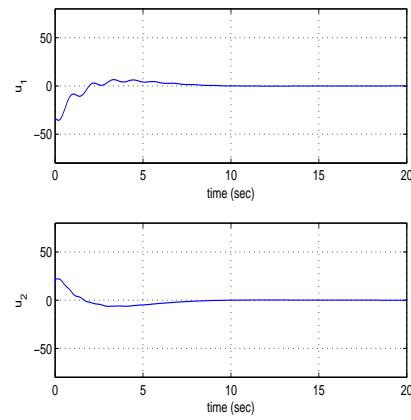


(b)

Figure 16: Tracking of setpoint 4 by the payload (a) trajectories in the OYZ plane followed by quadrotor 1 (red line) and quadrotor 2 (green line) and path followed by the cable-suspended payload (magenta line), (b) convergence of the state variables of the cable-suspended payload x_1 , x_3 and x_5 to the associated setpoints



(a)



(b)

Figure 17: Tracking of setpoint 4 by the payload: (a) convergence to zero of the tracking error of state variables x_1 , x_3 and x_5 of the cable-suspended payload (b) variation of control inputs u_1 , u_2 applied to the payload through the cables

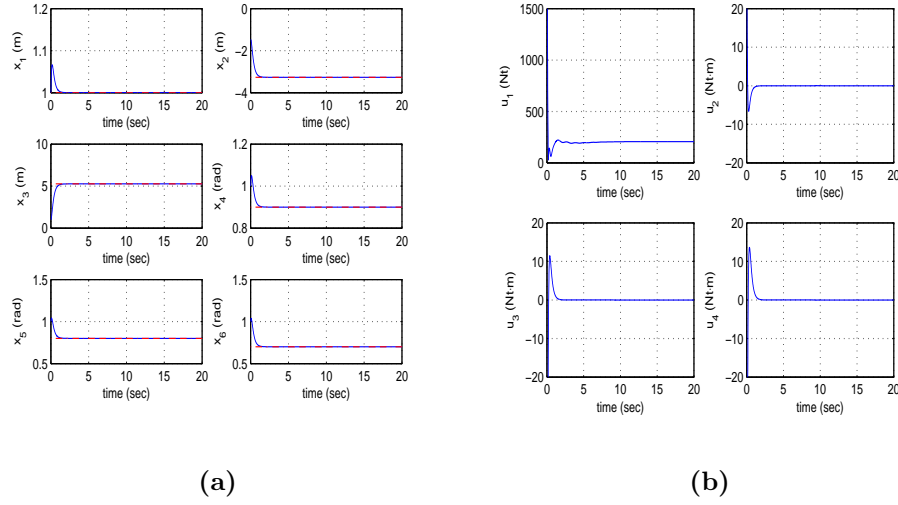


Figure 18: Tracking of setpoint 4 by the first UAV (a) convergence to setpoints (red line) for the state variables x_1 to x_6 of quadrotor 1 (blue line), (b) control inputs u_1 to u_4 of quadrotor 1 (blue line)

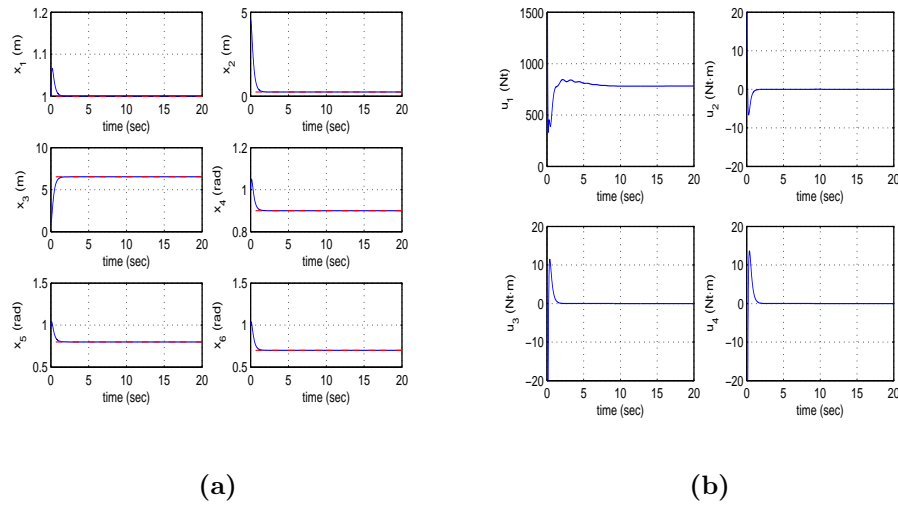
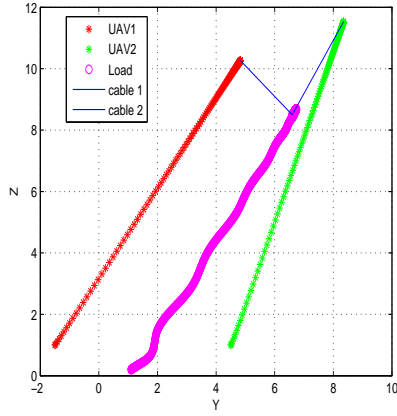
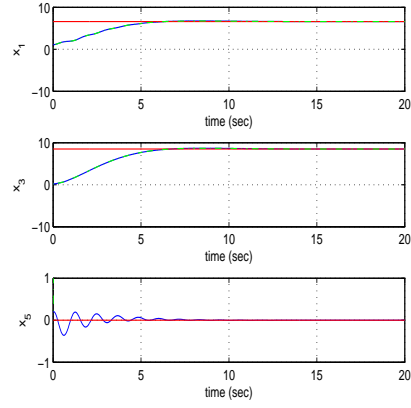


Figure 19: Tracking of setpoint 4 by the second UAV (a) convergence to setpoints (red line) for the state variables x_1 to x_6 of quadrotor 2 (blue line), (b) control inputs u_1 to u_4 of quadrotor 2 (blue line)

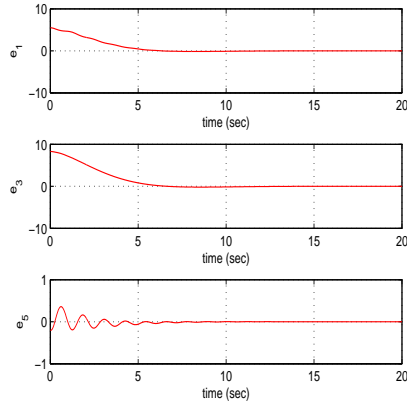


(a)

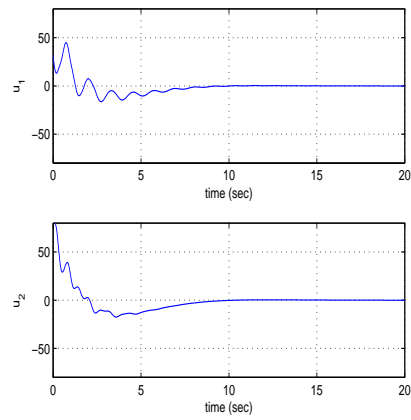


(b)

Figure 20: Tracking of setpoint 5 by the payload (a) trajectories in the OYZ plane followed by quadrotor 1 (red line) and quadrotor 2 (green line) and path followed by the cable-suspended payload (magenta line), (b) convergence of the state variables of the cable-suspended payload x_1 , x_3 and x_5 to the associated setpoints



(a)



(b)

Figure 21: Tracking of setpoint 5 by the payload: (a) convergence to zero of the tracking error of state variables x_1 , x_3 and x_5 of the cable-suspended payload (b) variation of control inputs u_1 , u_2 applied to the payload through the cables

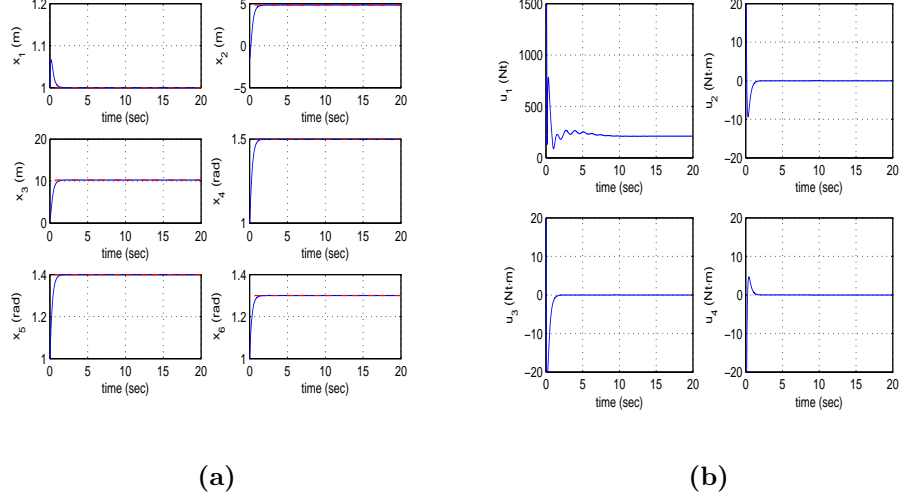


Figure 22: Tracking of setpoint 5 by the first UAV (a) convergence to setpoints (red line) for the state variables x_1 to x_6 of quadrotor 1 (blue line), (b) control inputs u_1 to u_4 of quadrotor 1 (blue line)

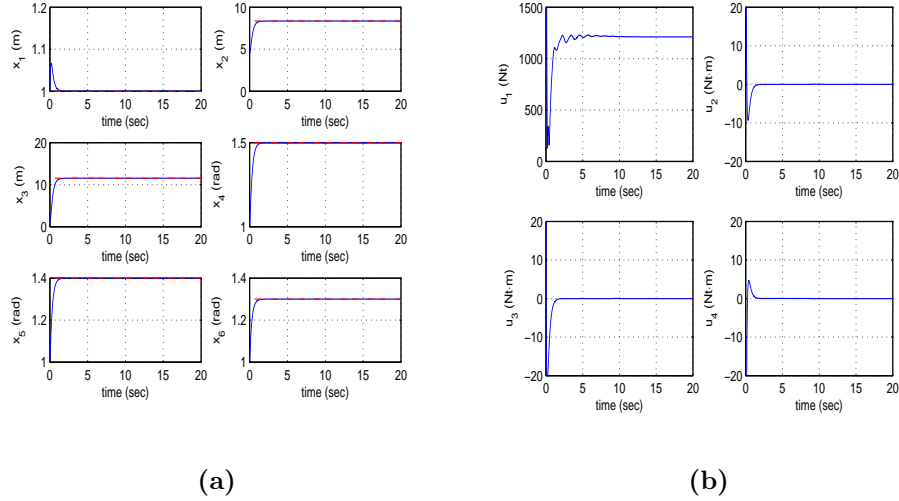
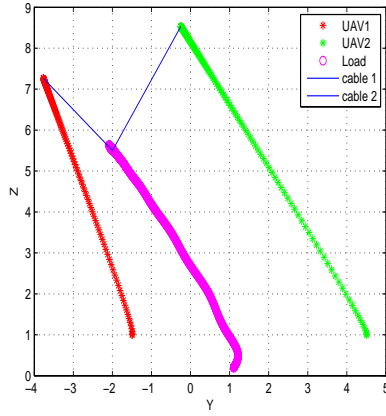
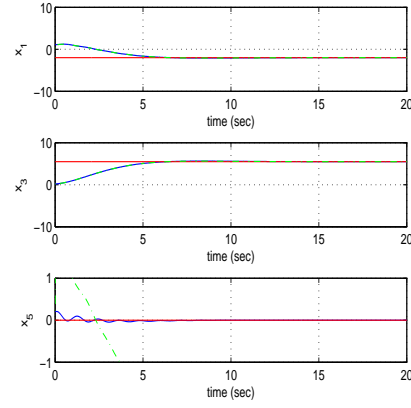


Figure 23: Tracking of setpoint 5 by the second UAV (a) convergence to setpoints (red line) for the state variables x_1 to x_6 of quadrotor 2 (blue line), (b) control inputs u_1 to u_4 of quadrotor 2 (blue line)

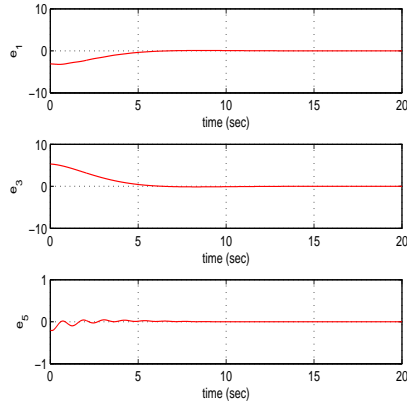


(a)

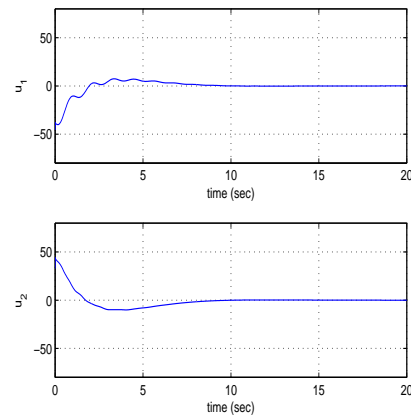


(b)

Figure 24: Tracking of setpoint 6 by the payload (a) trajectories in the OYZ plane followed by quadrotor 1 (red line) and quadrotor 2 (green line) and path followed by the cable-suspended payload (magenta line), (b) convergence of the state variables of the cable-suspended payload x_1 , x_3 and x_5 to the associated setpoints



(a)



(b)

Figure 25: Tracking of setpoint 6 by the payload: (a) convergence to zero of the tracking error of state variables x_1 , x_3 and x_5 of the cable-suspended payload (b) variation of control inputs u_1 , u_2 applied to the payload through the cables

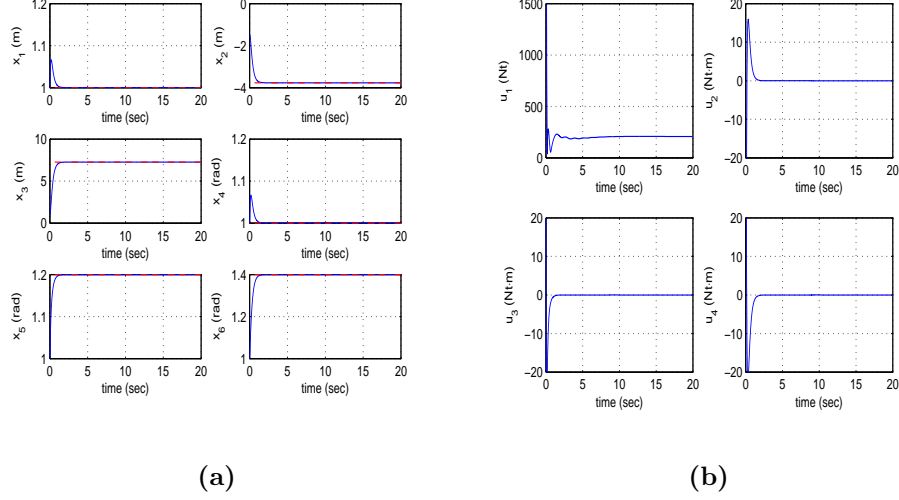


Figure 26: Tracking of setpoint 6 by the first UAV (a) convergence to setpoints (red line) for the state variables x_1 to x_6 of quadrotor 1 (blue line), (b) control inputs u_1 to u_4 of quadrotor 1 (blue line)

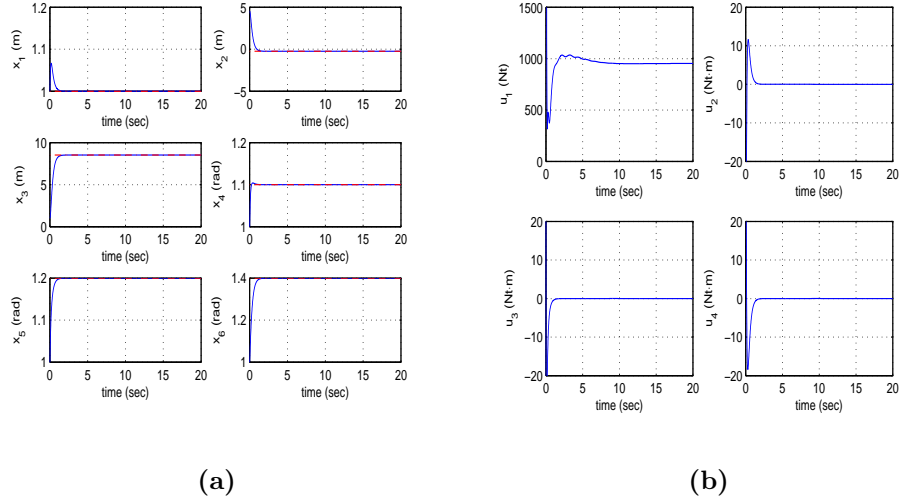
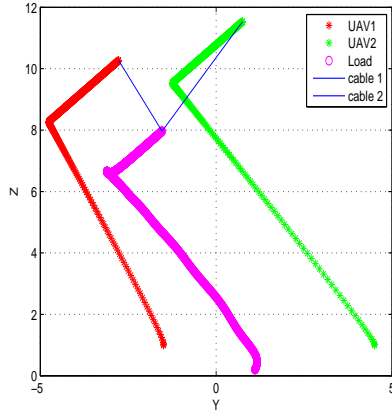
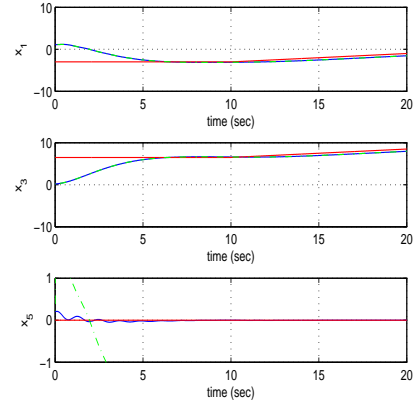


Figure 27: Tracking of setpoint 6 by the second UAV (a) convergence to setpoints (red line) for the state variables x_1 to x_6 of quadrotor 2 (blue line), (b) control inputs u_1 to u_4 of quadrotor 2 (blue line)

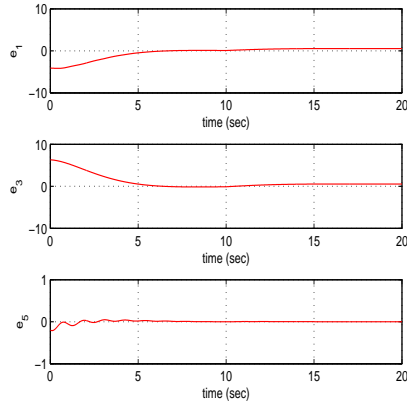


(a)

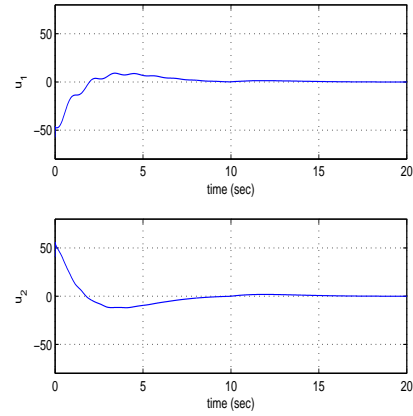


(b)

Figure 28: Tracking of setpoint 7 by the payload (a) trajectories in the OYZ plane followed by quadrotor 1 (red line) and quadrotor 2 (green line) and path followed by the cable-suspended payload (magenta line), (b) convergence of the state variables of the cable-suspended payload x_1 , x_3 and x_5 to the associated setpoints



(a)



(b)

Figure 29: Tracking of setpoint 7 by the payload: (a) convergence to zero of the tracking error of state variables x_1 , x_3 and x_5 of the cable-suspended payload (b) variation of control inputs u_1 , u_2 applied to the payload through the cables

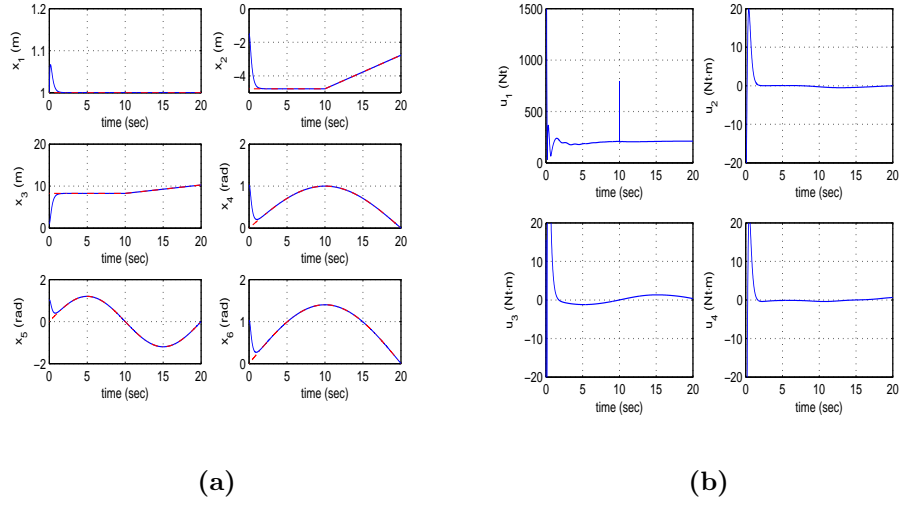


Figure 30: Tracking of setpoint 7 by the first UAV (a) convergence to setpoints (red line) for the state variables x_1 to x_6 of quadrotor 1 (blue line), (b) control inputs u_1 to u_4 of quadrotor 1 (blue line)

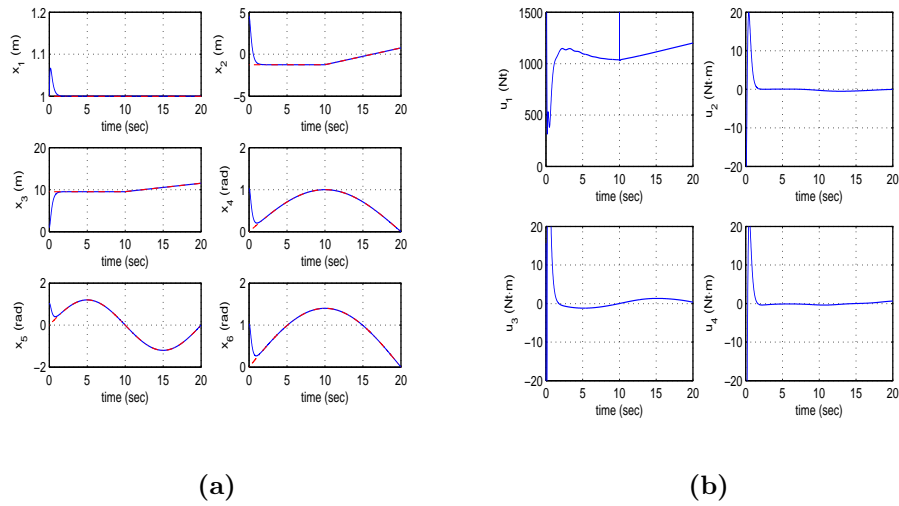
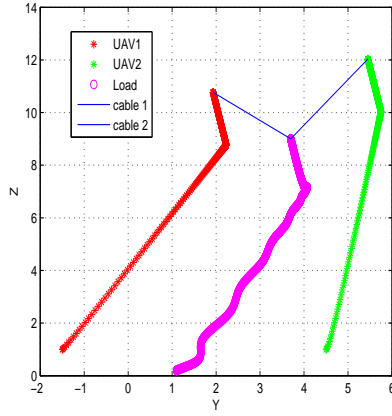
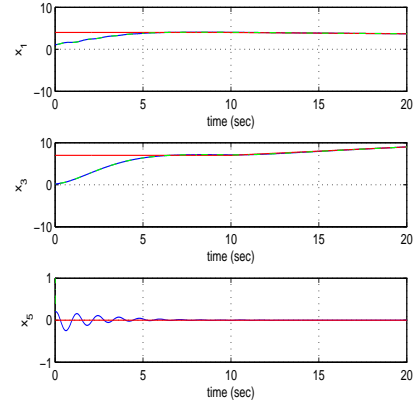


Figure 31: Tracking of setpoint 7 by the second UAV (a) convergence to setpoints (red line) for the state variables x_1 to x_6 of quadrotor 2 (blue line), (b) control inputs u_1 to u_4 of quadrotor 2 (blue line)

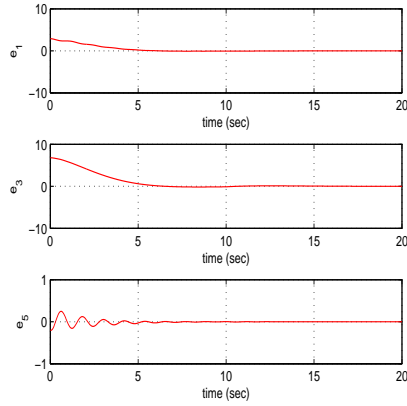


(a)

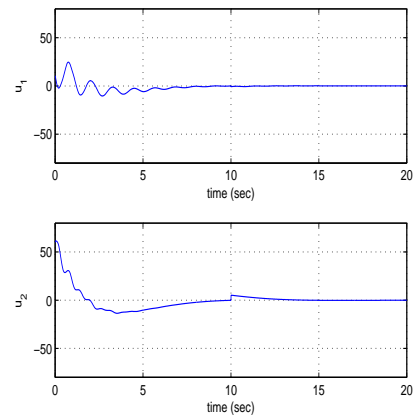


(b)

Figure 32: Tracking of setpoint 8 by the payload (a) trajectories in the OYZ plane followed by quadrotor 1 (red line) and quadrotor 2 (green line) and path followed by the cable-suspended payload (magenta line), (b) convergence of the state variables of the cable-suspended payload x_1 , x_3 and x_5 to the associated setpoints



(a)



(b)

Figure 33: Tracking of setpoint 8 by the payload: (a) convergence to zero of the tracking error of state variables x_1 , x_3 and x_5 of the cable-suspended payload (b) variation of control inputs u_1 , u_2 applied to the payload through the cables

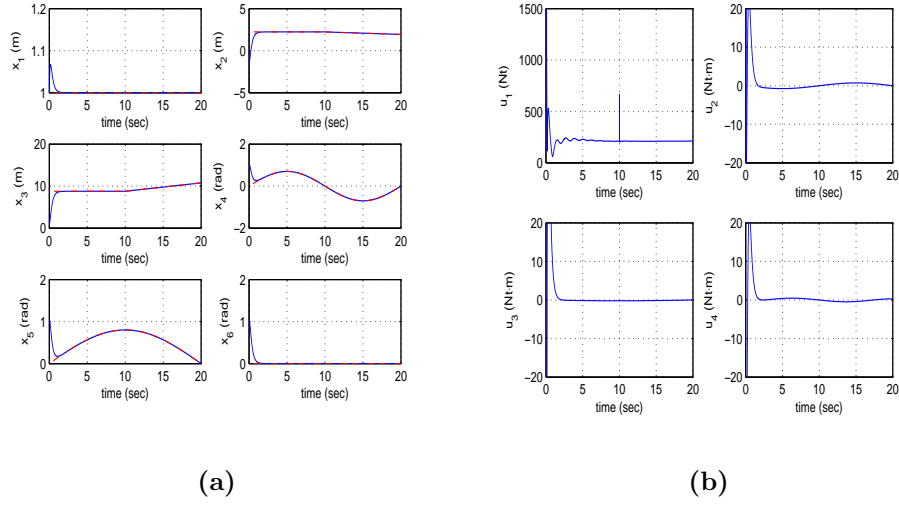


Figure 34: Tracking of setpoint 8 by the first UAV (a) convergence to setpoints (red line) for the state variables x_1 to x_6 of quadrotor 1 (blue line), (b) control inputs u_1 to u_4 of quadrotor 1 (blue line)

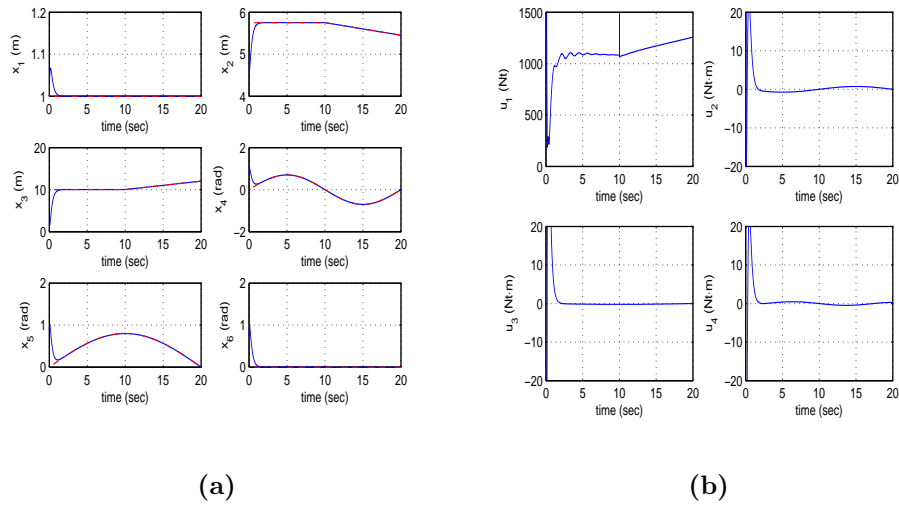


Figure 35: Tracking of setpoint 8 by the second UAV (a) convergence to setpoints (red line) for the state variables x_1 to x_6 of quadrotor 2 (blue line), (b) control inputs u_1 to u_4 of quadrotor 2 (blue line)

be repetitively solved at each time-step of the control algorithm. It was also proven through Lyapunov analysis that the values of the cables' forces which were computed through this procedure ensured global asymptotically stability for the payload and its precise placement at the desirable final position.

At a second stage, the cables' forces which were computed through the solution of the aforementioned optimal control problem were included as drag forces in the dynamic model of the two quadrotors. By solving the stabilization and flight-path tracking problem for these UAVs under the cable-induced drag forces one ensures that the payload is lifted and transported with cable-tensions that bring it to the desirable final position. To control the quadrotors and to achieve compensation of the drag forces from the cables, a multi-loop flatness-based control approach has been followed. In this flatness-based control in successive loops the nonlinear dynamic model of each drone was separated into cascading subsystems which were shown to satisfy differential flatness properties. For each subsystem of the state-space model of each drone a virtual control input was defined, capable of inverting the UAV's dynamics and of eliminating the associated tracking error. The control input which is actually applied to the initial nonlinear dynamic model of each drone was obtained from the last row of its state-space description. This control input incorporated in a recursive manner all virtual control inputs which were computed from the individual subsystems included in the initial state-space equation. The global stability properties of the new control method for the stabilization and flight-path following by each drone have been analytically proven with the use Lyapunov stability analysis, while exponential convergence has been also confirmed. The multi-loop flatness-based control method achieved fast and accurate tracking of the desirable flight trajectories of each quadrotor, under moderate variations of the control inputs. The method can be extended to the multi-UAV case and to 6-DOF payloads. In aggregate the nonlinear optimal and multi-loop flatness-based control scheme for dual UAV cooperative transportation of payloads ensured safe transportation and precise final positioning of the payload at any point in the drones' operating space. The quadrotors may have different dynamic models while the lengths of the cables may also be uneven.

Declarations:

Ethical Approval: This research work has not come against any ethical issues and does not include any experiments on humans or animals.

Conflict of Interest: The authors of this article state that, to their knowledge, no conflict of interest exists with third parties about the content and the results of the present manuscript.

Contribution: All authors have contributed to the concept, methodology, development and validation of the article's results. The contribution of each author to this research work is shown by the order of appearance of his name in the article's list of authors.

Availability of data and materials: Data associated with the article's results will be made available upon reasonable request.

Funding: (a) Gerasimos Rigatos has been partially supported by Grant Ref. 301022 "Nonlinear optimal and flatness-based control methods for complex dynamical systems" of the Unit of Industrial Automation, Industrial Systems Institute, Greece (b) Pierluigi Siano and Mohammed Al-Numay acknowledge financial support from the Researchers Supporting Project Number (RSP2024R150), King Saud University, Riyadh, Saudi Arabia.

Acknowledgement: Although the authors appreciate previous cooperation with other members of the academic community, they do not consider that a specific "acknowledgement" to third parties has to be included in this paper.

References

- [1] X. Zhang, F. Zhang and P. Huang, Formation planning after tethered UAV cooperative transportation with unknown payload and cable length, *IEEE Transactions on Automation Science and Engineering*, pp. 1-12, 2023.
- [2] X. Zhang, F. Zhang, P. Huang, J. Guo, H. Yu C. Pei and Y. Zhang, Self-triggered based coordinate control with low communication for thetethered multi-UAV collaborative transportation, *IEEE Robotics and Automation Letters*, vol. 6, no. 2, pp. 1559-1566, 2021.
- [3] A. Aliya and S. El-Ferik, Control of multiple UAV conveying slung load with obstacle avoidance, *IEEE Access*, vol. 10, pp. 62247-62257, 2023
- [4] D.K. Dourado-Villa, A. Santos Bradao, R. Carelli and M. Sarcinelli-Filho, Cooperative load transportation with two quadrotors using adaptive control, *IEEE Access*, vol. 9, pp. 129149-129158, 2021.
- [5] J.R. Goodman, T. Barkens and L.J. Colombo, Geometric control for load transportation with quadrotor UAVs by elastic cables, *IEEE Transactions on Control Systems Technology*, vol. 31, no. 6, pp. 2848-2862, 2023.
- [6] X. Jin and J. Hu, Adaptive cooperative load transportation by a team of quadrotors with multiple constraint requirements, *IEEE Transactions on Intelligent Transportation Systems*, vol. 24, no. 1, pp. 801-814, 2023
- [7] L.R. Salinas, J. Gimenez, D.C. Gandolfo, C.R. Rosales and R. Carelli, Unified motion control for multi-lift unmanned rotorcraft systems in forward flight, *IEEE Transactions on Control Systems Technology*, vol. 91, no. 4, pp. 1607-1621, 2023.
- [8] B. Shirari, N. Najofi and I. Izadi, Cooperative load transportation using multiple UAVs, *Aerospace Science and Technology*, Elsevier, vol. 84, pp. 158-169, 2019.
- [9] A. Mohladdi, Y. Zwairi, R. Almadhoun, T. Taha and D. Gan, Energy distribution in dual-UAV collaborative transportation through load sharing, *ASME Journal of Mechanisms and Robotics*, Paper No JMR-19-1378, pp. 1-14, 2020.
- [10] I.M. Belati Pizetta, A. Santos Brandao and M. Sarcinello-Filho, Avoiding obstacles in cooperative load transportation, *ISA Transactions*, Elsevier, vol. 91, pp. 253-261, 2019.
- [11] Y.M. Su, P. Bhawmick and A. Lanzan, A robust adaptive formation control methodology for networked multi-UAV systems with applications to cooperative payload, *Control Engineering Practice*, Elsevier, vol. 138, pp. 105608-105618, 2023.
- [12] O.L. Wang, G.J. Liu, P. Zhou, H.R. Shi and K.W. Zhang, Co-Tsi: Design and implementation of a 2-UAV cooperative transportation system, *Intl. Journal of Micro Air Vehicles*, Sage Publications, vol. 15, pp. 1-13, 2023.
- [13] B.E. Jackson, T.A. Howell, K. Shah, M. Schwager and Z. Morehester, Scalabel cooperative transport of cable-suspended loads with UAV using distributed trajectory optimization, *IEEE Robotics and Automation Letters*, vol. 5, no. 2, pp. 3368-3374, 2020.
- [14] Y.M. Tan, S. Lai, K. Wang and B.M. Chen, Cooperative control of multiple unmanned aerial systems with heavy-duty carrying, *Annual Reviews in Control*, Elsevier, vol. 46, pp. 44-57, 2018.
- [15] J. Geng and J.W. Langeloan, Cooperative transport of a slung load using load-leading control, *Journal of Guidance, Control and Dynamics*, vol. 43, no. 4, pp 1-19, 2020.
- [16] T. Chen and H.H.T. Liu, Cooperative transportation of a flexible payload using two quadrotors, *Journal of Guidance, Control and Dynamics*, vol. 44, no. 4, pp. 1-9, 2021.

- [17] K. Kotari, Z. Guo, T. Namerikawa and Z. Qu, Cooperative transport control by a multicopter system, *IET Control Theory and Applications*, vol. 15, pp. 861-875, 2021.
- [18] K. Klausen, C. Meissen, T.I. Fossen, M. Arcak and T.A. Johansen, Cooperative control for multirotor transporting an unknown suspended load under environmental disturbances, *IEEE Transactions on Control Systems Technology*, vol. 28, no. 2, pp. 653-660, 2020.
- [19] M. Sharma and S. Sundaram, A geometric control approach for multi-UAV cooperative payload transfer, *Nonlinear Dynamics*, Springer, vol. 111, pp. 10077-10096, 2023.
- [20] J. Goodman and L. Colombo, Geometric control of two quadrotors carrying a rigid rod with elastic cables, *Journal of Nonlinear Science*, Springer, vol. 32, no. 65, pp. 1-31, 2022.
- [21] G. Li, R. Ge and F. Loianno, Cooperative transportation of cable-suspended payloads with MAVs using monocular vision and inertial sensing, *IEEE Robotics and Automation Letters*, vol. 6, no. 3, pp. 5316-5325, 2021.
- [22] J. Gimenez, D/C/ Gandolfo, L.R. Salinas, C. Rosales and R. Carelli, Multi-objective control for cooperative payload transport with rotorcraft UAS, *ISA Transactions*, Elsevier, vol. 80, pp. 491-602, 2018.
- [23] M. Dookhan, M. Kabganian and A. Azimi, Cooperative payload transportation with real-time formation control of multi-quadrotors in the presence of uncertainty, *Journal of the Franklin Institute*, Elsevier, vol. 360, pp. 1284-1307, 2023.
- [24] F. Pierri, M. Nigro, G. Muscolo and F. Caccavale, Cooperative manipulation of an unknown object via omnidirectional unmanned aerial vehicle, *Journal of Intelligent and Robotic Systems*, Springer, vol. 100, pp. 1635-1649, 2020.
- [25] C. Masone and P. Stepagno, Shared control of an aerial cooperative transportation system with a cable-suspended payload, *Journal of Intelligent and Robotic Systems*, Springer, vol. 113, no. 40, pp. 1-29, 2021.
- [26] D. Sanalitra, H.J. Savino, M. Tognon, J. Cortes and A. Franchi, Full-base manipulation control of a cable-suspended load with multiple UAVs under uncertainties, *IEEE Robotics and Automation Letters*, vol. 5, no. 2, pp. 2185-2191, 2020.
- [27] A.E. Jimenez-Cano, D. Sanalitra, M. Tognon, A. Franchi and J. Cortes, Precise Cable-Suspended Pick-and-Place with an Aerial Multi-robot System: A Proof of Concept for Novel Robotics-Based Construction Techniques, *Journal of Intelligent and Robotic Systems*, Springer, vol. 105, no. 68, pp. 1-13, 2023.
- [28] G. Rigatos and K. Busawon, *Robotic manipulators and vehicles: Control, estimation and filtering*, Springer, 2018.
- [29] G. Rigatos and E. Karapanou, *Advances in applied nonlinear optimal control*, Cambridge Scholars Publishing, 2020.
- [30] G. Rigatos, M. Abbaszadeh, M.A. Hamida and P.Siano, *Intelligent control for electric power systems and electric vehicles*, monograph in press, 2023.
- [31] G.G. Rigatos and S.G. Tzafestas, *Extended Kalman Filtering for Fuzzy Modelling and Multi-Sensor Fusion*, *Mathematical and Computer Modelling of Dynamical Systems*, Taylor & Francis, vol. 13, pp. 251-266, 2007.
- [32] M. Basseville and I. Nikiforov, *Detection of abrupt changes: Theory and Applications*, Prentice-Hall, 1993.

- [33] G. Rigatos and Q. Zhang, Fuzzy model validation using the local statistical approach, *Fuzzy Sets and Systems*, Elsevier, vol. 60, no. 7, pp. 882-904, 2009.
- [34] G. Rigatos, M. Abbaszadeh, P. Siano, *Control and estimation of dynamical nonlinear and partial differential equation systems: Theory and Applications*, IET Publications, 2022
- [35] G.J. Toussaint, T. Basar and F. Bullo, H_∞ optimal tracking control techniques for nonlinear under-actuated systems, in *Proc. IEEE CDC 2000, 39th IEEE Conference on Decision and Control*, Sydney Australia, 2000.
- [36] G. Rigatos, *Nonlinear control and filtering using differential flatness theory approaches: Applications to electromechanical systems*, Springer, 2016
- [37] J. Levine, *Analysis and Control of Nonlinear Systems: A flatness-based approach*, Springer 2009.
- [38] S. Riachy, M. Fliess, C. Join and J.P. Barbot. Vers une simplification de la commande non linéaire : l'exemple d'un avion à décollage vertical. Sixième Conférence Internationale Francophone d'Automatique, CIFA 2010, Jun 2010, Nancy, France
- [39] M. Fliess and H. Mounier, Tracking control and π -freeness of infinite dimensional linear systems, In: G. Picci and D.S. Gilliam Eds., *Dynamical Systems, Control, Coding and Computer Vision*, vol. 258, pp. 41-68, Birkhäuser, 1999.
- [40] J. Villagra, B. d'Andrea-Novet, H. Mounier and M. Pengov, Flatness-based vehicle steering control strategy with SDRE feedback gains tuned via a sensitivity approach, *IEEE Transactions on Control Systems Technology*, vol. 15, pp. 554- 565, 2007.
- [41] S. Bououden, D. Boutat, G. Zheng, J.P. Barbot and F. Kratz, A triangular canonical form for a class of 0-flat nonlinear systems, *International Journal of Control*, Taylor and Francis, vol. 84, no. 2, pp. 261-269, 2011.
- [42] L. Menhour, B. d'Andre'a-Novet, M. Fliess and H. Mounier, Coupled nonlinear vehicle control: Flatness-based setting with algebraic estimation techniques, *Control Engineering Practice*, Elsevier, vol. 22, pp. 135–146, 2014
- [43] F. Nicolau, W. Respondek and J.P. Barbot, How to minimally modify a dynamical system when constructing flat inputs, *International Journal of Robust and Nonlinear Control*, J. Wiley, 2022.
- [44] C. Letelier and J.P. Barbot, Optimal flatness placement of sensors and actuators for controlling chaotic systems, *Chaos*, AIP Publications, vol. 31, no. 10, article No 103114, 2021.
- [45] H. Sira-Ramirez and S. Agrawal, *Differentially Flat Systems*, Marcel Dekker, New York, 2004.
- [46] J. Lévine, On necessary and sufficient conditions for differential flatness, *Applicable Algebra in Engineering, Communications and Computing*, Springer, vol. 22, no. 1, pp. 47-90, 2011.
- [47] F. Nicolau, W. Respondek and J.P. Barbot, Construction of flat inputs for mechanical systems, 7th IFAC Workshop on Lagrangian and Hamiltonian methods for nonlinear control, Berlin, Germany, Oct. 2021
- [48] J.O. Limaverde Filho, E.C.R. Fortaleza and M.C.M. Campos, A derivative-free nonlinear Kalman Filtering approach using flat inputs, *International Journal of Control*, Taylor and Francis 2021.
- [49] J.P. Barbot, M. Fliess and T. Floquet, An algebraic framework for the design of nonlinear observers with unknown inputs, *IEEE CDC 2007, IEEE 46th Intl. Conference on Decision and Control*, New Orleans, USA, Dec. 2007

- [50] G. Rigatos, M. Abbaszadeh, K. Busawon, L. Dala and J. Pomares, Flatness-Based Control In Successive Loops For Autonomous Quadrotors, ASME Journal of Dynamic Systems, Measurement and Control, pp. 1-19, 2023
- [51] G. Rigatos, M. Abbaszadeh and J. Pomares, Flatness-based control in successive loops for electropneumatic actuators and robots, IFAC Journal of Systems and Control, Elsevier, vol. 25, pp. 100221-100243, 2023.
- [52] G. Rigatos, P. Siano and N. Zervos, A new concept of flatness-based control of nonlinear dynamical systems, IEEE INDIN 2015, 13th IEEE Intl. Conf. on Industrial Informatics, Cambridge, UK, July 2015
- [53] G. Rigatos, P. Siano, S Ademi and P. Wira, Flatness-based control of DC-DC converters implemented in successive loops, Electric Power Components and Systems, Taylor and Francis, vol. 46, no. 6, pp. 673-687, 2018.
- [54] G. Rigatos, Flatness-based embedded control in successive loops for spark ignited engines, Journal of Physics, IOP Publications, Conference Series No 659, 012019, IFAC ACD 2015, Proc. of the 12th European Workshop on Advanced Control and Diagnosis.
- [55] G. Rigatos, P. Wira, M. Abbaszadeh and J. Pomares, Flatness-based control in successive loops for industrial and mobile robots, IEEE IECON 2022, IEEE 48th Annual Conference of the Industrial Electronics Society, Brussels, Belgium, Oct. 2022